Magmatic processes beneath the volcanic island of Saba

Marloes Zomerdijk
Student number: 2074699
Research project master Solid Earth
February 2015
Vrije Universiteit Amsterdam

Abstract

The volcanic island of Saba is located in the Caribbean Sea and is part of the Lesser Antilles volcanic arc. The andesitic domes of Saba preserve a lot of andesitic hostrocks as well as mafic enclaves. These rocks record the evolution of the magmas in space and time. In this project the magmatic processes beneath the island of Saba were studied. Knowledge of the magmatic processes beneath volcanoes are highly relevant for understanding the processes that build volcanoes, investigating volcanic cycles and better prediction of volcanic eruptions. Samples were obtained from 56 different sample locations and were studied in terms of their major- and minor element compositions. $^{87}Sr/^{86}Sr$ isotope ratios were obtained for 8 whole rock samples and 10 picked plagioclase samples. The plagioclase data show that the large unaltered fraction which is found both in hostrocks as in enclaves all have the same source. There is abundant macroscopic, microscopic and geochemical evidence of mixing. AFC processes could possibly also explain some of the differentiation trends. The assimilant probably consists of old arc crust material. Saba rocks are hardly influenced by sediments.

Contents

Chapter 1: Introduction

The volcanic island of Saba is located in the Caribbean Sea and is part of the Lesser Antilles volcanic island arc. This volcanic arc is a 850-km-long chain of volcanoes formed by the west-northwest subduction of the Atlantic plate beneath the Caribbean plate at a current rate of 2-4 cm yr^{-1} (Macdonald and Holcombe, 1978). The volcanic arc can be divided into two arcs: one old arc in the east which is composed of Eocene to Oligocene igneous rocks and one active arc in the west which evolved in the late Miocene/early Pliocene. Saba forms the northernmost volcano of the active arc. Volcanism on Saba can be subdivided into four stages. The first stage (~500.000 years ago) of volcanic activity was characterized by the formation of Pelean domes and dome flows. The second stage (400.000-100.000 years ago) consisted of Plinian-style activity. The third stage is characterized by the formation of the horseshoe-shaped crater which is probably caused by a sector collapse. In the last stage this horseshoe-shaped structure has been filled in with pyroclastic material and andesitic domes. There are indications that the last eruption of Saba probably took place around 1600, just prior to European settlement (Roobol and Smith, 2004).

Magmatic rocks experience differentiation processes in a magma chamber prior to their emplacement at the surface. These processes modify the chemical composition of the primary magma which is produced by partial melting of the source; the subducting oceanic slab. The main processes are fractional crystallization, magma mixing and assimilation. In most cases, a mixture of these processes occurs.

Field observations show abundant and clear evidence of mixing of a more mafic magma with a more felsic magma (see figure 10). Therefore the research questions of this study are:

1. Is there one parental mafic magma, or are there more than one mafic magma types?
2. Does the composition of the felsic and mafic magma types change over time?
3. Is the felsic magma related to the mafic magma by fractional crystallization?
4. Is the felsic magma influenced by assimilation- and fractional crystallization processes?

Knowledge of the magmatic processes beneath volcanoes are highly relevant for understanding the processes that build volcanoes, investigating volcanic cycles and better prediction of volcanic eruptions. This is especially important in the case of Saba because the volcano is seen as dormant and the main village is located in a valley. Field observations showed different signals.

Samples were collected from 56 different locations of the island. Care was taken by sampling both mafic enclaves as hostrocks. All the samples were powdered and analyzed with XRF for major and trace-elements. 10 whole rock samples and 8 picked plagioclase samples were used for isotope analysis. The obtained data shows that there is a complex magmatic system beneath Saba.

Chapter 2: Geological setting

2.1 Introduction

The volcanic island of Saba is located in the Caribbean Sea between Puerto Rico in the North and Venezuela in the South. Saba is part of the Lesser Antilles volcanic island-arc chain (Figure 1). This Island-arc is a 850-km-long curved chain of volcanoes formed by the west-northwest subduction of the Atlantic plate beneath the Caribbean plate. The convergence rate is low, estimates vary from 2 to 4 cm yr^{-1} (Macdonald and Holcombe, 1978). The active volcanic chain consists of the islands; Grenada, Grenadines, St. Vincent, St Lucia, Martinique, Dominica, Les Saintes, Basse Terre of Guadeloupe, Montserrat, Redona, Nevis, St. Kitts, St. Eustatius and Saba. This chapter describes the regional tectonics of the Lesser Antilles and the variations in volcanism along the arc. At the end of this chapter the volcanic island of Saba is discussed in more detail.

2.2 Tectonics of the Lesser Antilles

As stated above, the Lesser Antilles Island arc results from the west-northwestward subduction of old Atlantic oceanic crust beneath the Caribbean plate with a convergence rate of 2 cm yr^{-1}. The Lesser Antilles volcanic arc can be divided into two arcs: one old arc in the east which is composed of Eocene to Oligocene igneous rocks and one active arc in the west which evolved in the late Miocene/early Pliocene. Martinique forms the southern tip of the separation. Islands south of Martinique belong both to the old volcanic arc as to the new volcanic arc as shown in Figure 1. The active chain is often referred as the Volcanic Caribees whereas the older arc is referred as Limestone Caribees. The two arcs diverge to the north with a maximum divergence of 50 km expressed by the Kallinago depression east of Saba (Figure 1) (Roobol and Smith, 2004).

In most volcanic arcs, trough time volcanism will migrate towards the trench because of a steepening of the subducting slab. In case of the northern Lesser Antilles, the migration of the volcanic front occurred away from the trench in westward direction. The westward shift of the volcanic front is thought to be related to the attempted subduction of aseismic ridges which caused a flattening of the subducting slab (Bouysse and Westercamp, 1990). These aseismic ridges exist north of the island St. Lucia on the eastern side and run northwest-southeast. From north to south, they are named the Barracuda ridge, Tiburon ridge and the Saint Lucia ridge (Figure 1). According to the Bouysse and Westercamp (1990) model, the buoyancy of the subducting plate is temporarily interrupted when the ridge reached the subduction zone which caused a decrease in magmatic production and volcanism. After that the ridge-arc collision caused regional uplift. When subduction continued the dip angle of the slab became shallower because of the extra buoyancy of the ridge. Eventually this led to a shift of the volcanic chain towards the back-arc region. Evidence supporting this model is that a large part of the northeast fore-arc region has been uplifted in Quaternary times. An alternative model suggests that the eastward movement of the Caribbean plate has been disturbed by the South American continental margin in the south. Therefore eastward movement of the plate has resulted in more displacement in the north (Germa et al., 2011).

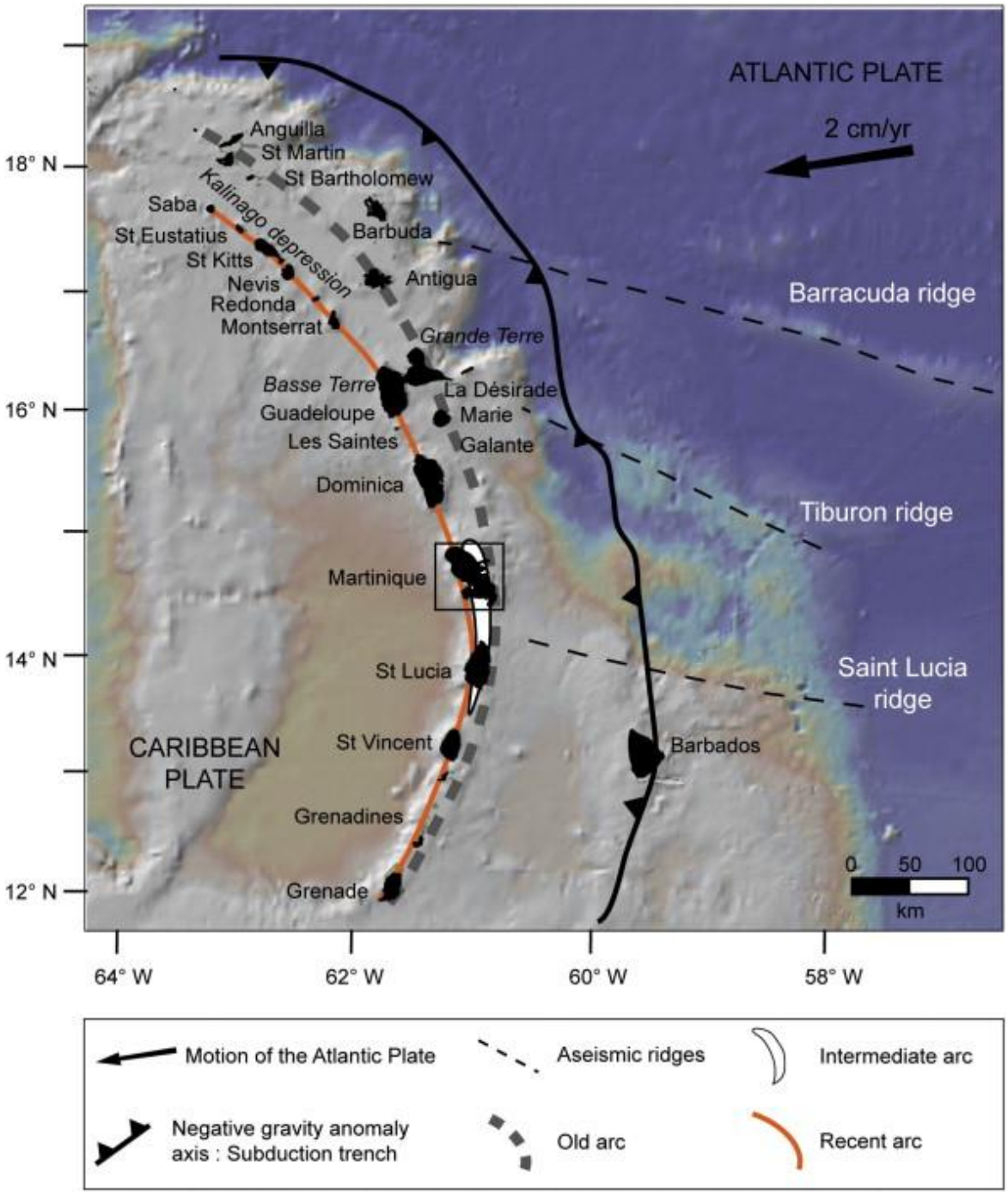

Figure 1: Map of the Lesser Antilles volcanic island arc showing the Volcanic Caribees (old and new arc), the aseismic ridges and the Kalinago depression (Germa et al., 2011).

West of the island arc, Westbrook et al (1984) located faults from seismic reflection profiles. The faults are parallel and transverse to the arc which indicates a horst and graben structure (Roobol and Smith, 2004). The fore-arc region in the east is complex. The width ranges from 150 km in the north to 450 km in the south. The region is marked by a deformation front, characterized by folding and thrusting. In the north, the fore-arc reaches depths over 8 km. These depths shallow towards the south (Macdonald et al., 2000).

There is a large variation in sediment thickness along the Lesser Antilles Arc. Most of the sediments are terrigenous and transported via the Orinoco River to the ocean floor of the Atlantic plate (Macdonald et al., 2000). In the southern part of the arc the sediments reach a thickness up to 4 km. The thickness of the sediments decreases towards the north to only a few hundred meters (Macdonald et al., 2000). The earlier mentioned aseismic ridges act as barriers for the sediments and therefore significantly decrease the amount of sediment carried northward. Pelagic sediments dominate the coast of the northernmost islands. The amount of sediment offscraping of the Atlantic plate due to subduction is so large that the accretionary prism rises above sea level which is expressed as the island of Barbados east of the Grenadines (Figure 1).

In the period from 1978-1984, Wadge and Shepherd (1984) used the hypocenters of earthquakes to reconstruct the benioff zone which is shown in Figure 2. Note that the benioff zone is segmented in two parts; one south of Martinique and one north of Martinique which is also the location of the shift in the volcanic front. The northern segment trends 330° with a dip of 50-60°. The southern segment trends 20° with a dip of 45-50°.

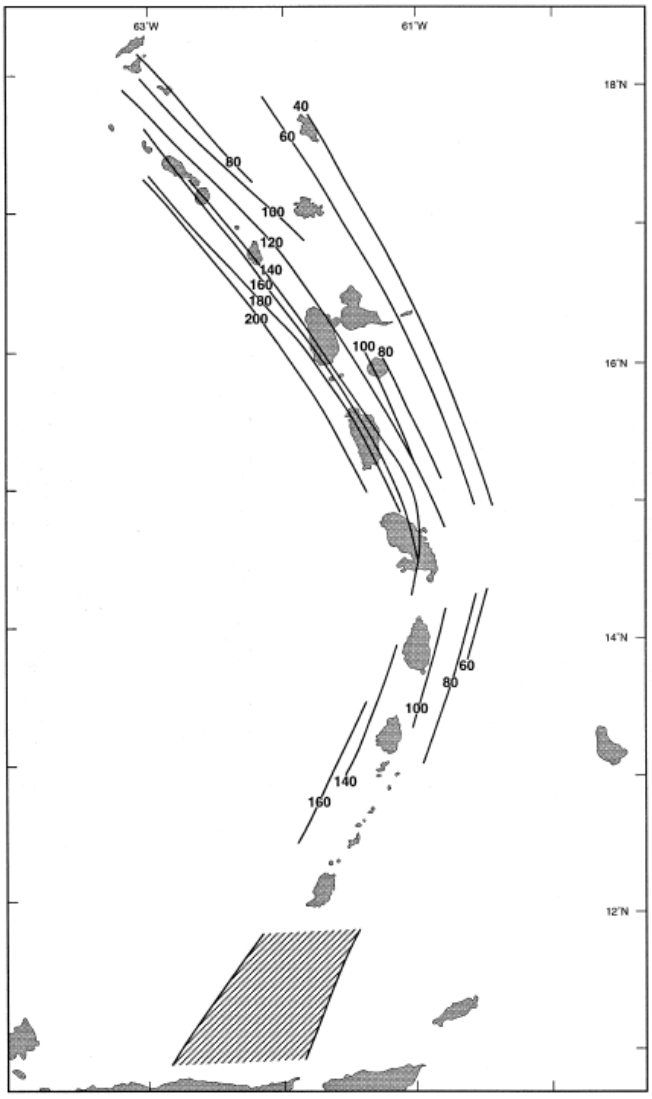

Figure 2: position of the Benioff zone beneath the Lesser Antilles. Contours have 20 km depth intervals.
(Wadge and Shepherd, 1984)

The submarine Aves Ridge is similar in dimensions and shape as the Lesser Antilles arc. It is located west of the Lesser Antilles and is separated from the Lesser Antilles by the Grenada basin. The ridge has a north-south direction, is 600 km long and rises 1000-2000 meters above the Venezuela basin on the west and the Grenada basin on the east. The Aves Ridge has a width of over 100 km in east-west direction. Drilling results indicate that the Aves Ridge was an active volcanic arc during the upper Cretaceous and early Paleocene (Roobol and Smith, 2004),

The Kallinago depression lies between the active and the extinct volcanic arcs north of Guadeloupe. From Anguilla to Guadeloupe it has a length of 250 km. The broadest and deepest parts are located between Saba/St. Eustatius and Anguilla where the with at sea level is 50 km and the bottom width is 20 km. The Kallinago depression appears to be intermittent by Guadeloupe but the Arawak Valley seems to be a continuation of the Kallinago depression because it has a similar orientation. Westbrook et al (1984) interpreted the structures as a graben structure which probably originated in a back arc position.

The Saba bank lies 5 km southwest of Saba (**Fout! Verwijzingsbron niet gevonden.**). It is a submerged carbonate platform of 2680 km² which stands around 1000 m above the surrounding sea floor. Water depths vary from 20 m in the south to 40 m in the north. Four major stratigraphic units were obtained from seismic profiles and two boreholes (Warner, 1990). The lower unit consists of an andesitic porphyry which is dated at 64,5 Ma. The second unit consists of a thin quartz conglomerate which is overlain by Eocene reef limestones or clay and sandstone beds of turbiditic origin. The third unit consists of volcaniclastic rocks consisting of conglomerates, sandstones and siltsones of upper Eocene to lower Miocene age. The upper unit consists of platform limestones of Middle Miocene to early Pliocene age (Roobol and Smith, 2004). Underlying the andesitic porphyry lies a thick sedimentary sequence that can go back to early Cretaceous age. During the late Cretaceous, Saba Bank is believed to have occupied a backarc position on the Aves Swell volcanic arc. This arc was part of the Greater Antilles volcanic arc which also included Cuba and Puerto Rico (Warner,1990).

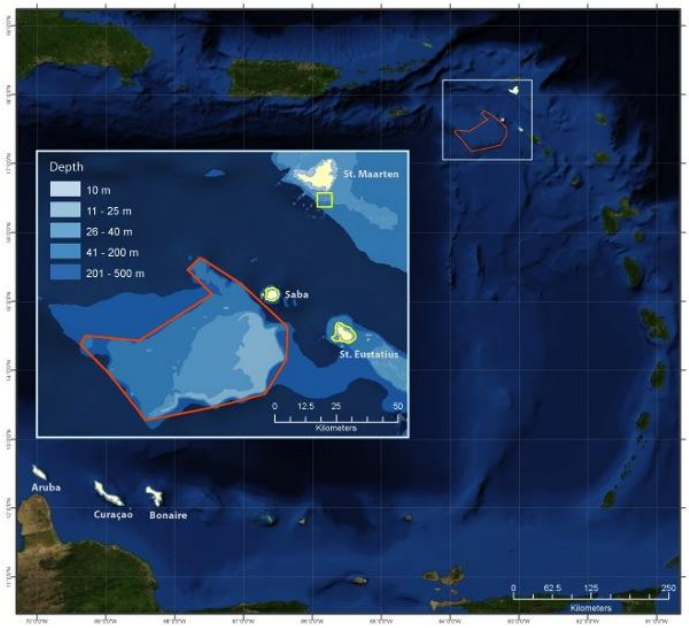

Figure 3: Saba bank (http://www.dcnanature.org/saba-bank)

2.3 Along-arc variations

The Lesser Antilles island arc can be divided into three groups based on petrography; the northern group is formed by Saba, St. Eustatius, St. Kitts, Nevis, Redona and Montserrat, the central group

consists of Guadeloupe, Dominica, Martinique and St. Lucia, the southern group is formed by St. Vincent, Grenadines and Grenada (Macdonald et al., 2000).

The dominant rock type in the northern group is andesite, with minor amounts of dacite. Some rhyolites have also been found on St. Kitts and St. Eustatius but these are rare. The volumes of basalt are low (e.g. 10% on St. Kitts, 3% on Montserrat). On Saba basalts are found as blocks in pyroclastic deposits (Macdonald et al.,2000).

The dominant rock type in the central group is andesite with some basalts and dacites. Rhyolites are also rare in this group. This group includes the largest islands in the arc and the total volume of erupted volcanic products is larger than in the other groups. Over the past 0,1 Ma the volcanic production has been higher than in other parts of the arc (Macdonald et al., 2000).

On St. Vincent mainly basalts and basaltic andesites are found. Andesites are observed as components in mixed magma rocks. The rocks on Grenada and the Grenadine islands are more complex, and range from picritic and ankaramitic basalts through andesites and rare dacites. Magnesium rich rocks found on these islands are silica-undersaturated (Macdonald et al., 2000).

Turner et al (1996) noted that there is a north-south along-arc progression from tholeiitic through calc-alkaline to alkaline lavas. This progression is accompanied by increasing $^{87}Sr/^{86}Sr$ and $^{207}Pb/^{204}Pb$ and decreasing $^{143}Nd/^{144}Nd$. They subdivided their isotopic data into four groups showed in Figure 4.

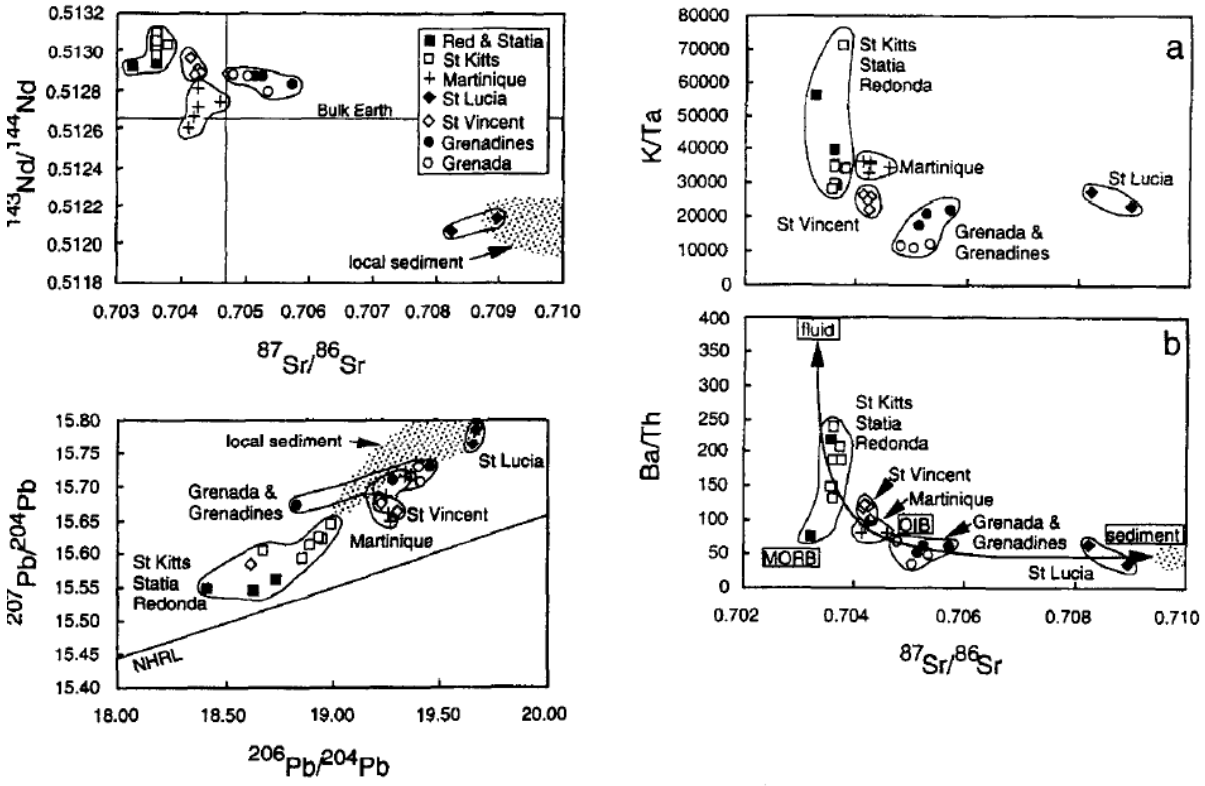

Figure 4: $^{87}Sr/^{86}Sr$ vs $^{143}Nd/^{144}Nd$ and $^{207}Pb/^{204}Pb$ vs $^{206}Pb/^{204}Pb$, illustrating the overall increase in $^{87}Sr/^{86}Sr$, $^{207}Pb/^{204}Pb$ and $^{206}Pb/^{204}Pb$ and decrease in $^{143}Nd/^{144}Nd$ southwards along the arc. K/Ta vs $^{87}Sr/^{86}Sr$ shows that the highers LIL/HFSE ratios are preserved in the most depleted lavas from the northern Lesser Antilles. Ba/Th vs $^{87}Sr/^{86}Sr$ shows a good hyperbolic correlation for the Lesser Antilles lavas. Low Ba/Th and high $^{87}Sr/^{86}Sr$ corresponds to subducted sediment and crustal contamination (from Turner et al 1996, their figures 3 and 4).

2.4 Saba

The volcanic Island of Saba(coordinates 17° 38' N, 63° 14' W) forms the northernmost volcano of the active volcanic arc. It is located 30 km southwest of Saint Martin. Saba is a small island with an average width of 4,5 kilometers and a total area of 13 square kilometers. Mount Scenery is the highest peak on the island and rises 887 meters above sea level. Other peaks are represented by Pelean domes (Roobol and Smith, 2004).

The lavas of Saba belong to the medium-K and low-Ca calc-alkaline series. They form a single magma series ranging from basalt to dacite. Rocks on the island appear to be related by fractional crystallization with andesite being the most abundant rock type. The rocks probably do not represent primary magmas derived by partial melting of the mantle wedge but magma that has been altered by fractional crystallization. Orthopyroxene is absent in the Saba lavas, instead amphiboles are found. This suggests that magma crystallization took place under conditions were high water contents are present (Roobol and Smith, 2004). Lithic fragments of limestone have been reported in the pyroclastic deposits and as inclusions in andesitic lava blocks. From these fragments can be concluded that limestone platforms are located beneath the volcano (Roobol and Smith, 2004). More information about the petrology of Saba can be found in other chapters.

Saba is a single volcano rising to a central peak which is dome-capped. The longest axis of the island runs perpendicular to the axis of the island arc. This is unusual because the remaining islands of the Lesser Antilles all have an axis parallel to the axis of the island arc. The most accepted explanation for this is that Saba lies on a fault orientated perpendicular to that of the volcanic arc (Roobol and Smith, 2004).

In Figure 5 the topography and bathymetry around Saba to a depth of 500 mis shown. Overall, the submarine contours are equally divided around the island except in the west. This suggests that the island can be regarded as one single volcanic complex. The submarine mountain west of the island has depths of 300 meters to 23 meters below sea level. Because the dimensions and morphology of this mountain are the same as the Pelean domes exposed on Saba, it seems logical that this mountain is also a parasitic dome. The 50 m submarine contour defines a shallow-water platform on the western and northern flanks of the island. Like the earlier mentioned long axis of the island, the platform is located reverse of what is commonly found on islands of the Lesser Antilles. This morphology is probably a result of the distribution and spacing of lava domes and flows. The volcanic rocks form a host for the limestone platforms (Roobol and Smith, 2004).

On Saba a horseshoe-shaped structure can be found, it is 2.5 km in length, 1.2 km width and 0.38 km deep it is opening towards the southwest. The horseshoe-shaped structure encloses the central vent zone of the volcano which continues to act as a crater. In the Lesser Antilles seven other horseshoe-shaped structures have been recognized (Roobol and smith, 2004). With the exception of Martinique, all of these structures open towards the southwest and lie contiguous to the steepest submarine slopes. Therefore Roobol et al. (1983) suggested a structure forming mechanism of gravitational collapse which could be triggered by inflation of the volcano and/or earthquakes. This theory is in agreement with what happened with the eruption of Mount Saint Helens in 1980. Dome growth and pyroclastic products have filled the crater of Saba for a large part, leaving only the outer part of the sector collapse scar exposed.

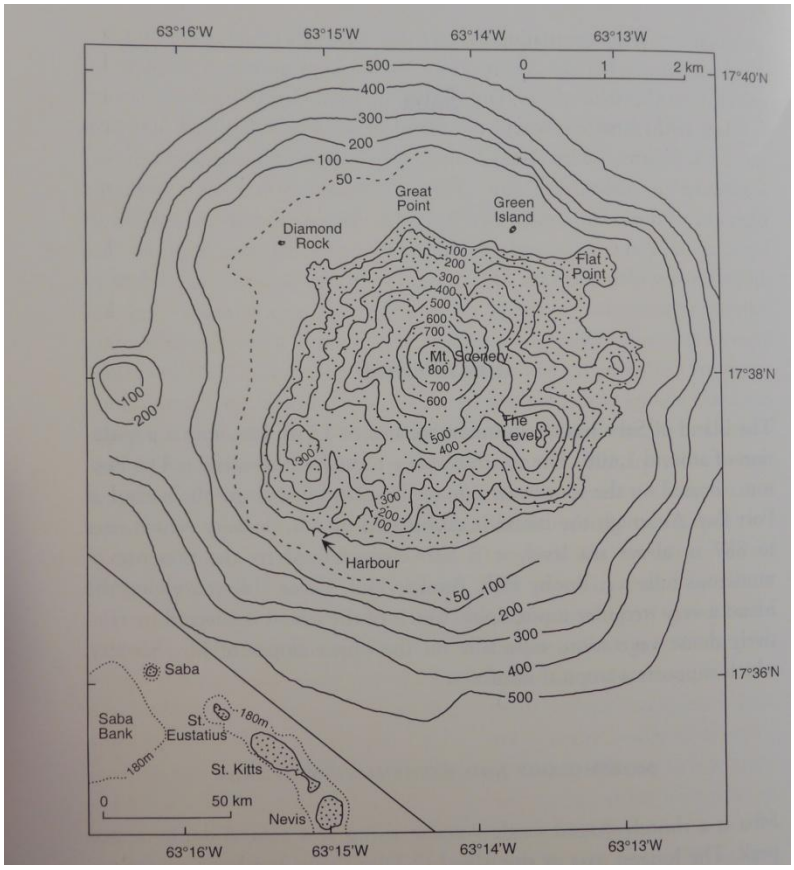

Figure 5: Topography and bathymetry of Saba. (Roobol and Smith, 2004)

The structural evolution of Saba can be subdivided into four stages which are illustrated in Figure 6 (Roobol and Smith, 2004). Stage 1 occurred about half a million years ago when the island was formed as a complex of andesitic Pelean domes and dome flows surrounded by pyroclastic material. Stage 2 happened between 400.000 and 100.000 years ago. In this stage Plinian-style activity occurred with andesitic to dacitic pumice fall and flow deposits, Pelean activity was also still present in this stage. Stage 3 started 100.000 years ago. In this stage the horseshoe-shaped crater formed. This event exposed the hydrothermally altered core of the volcano located at the village 'The Bottom'. Stage 4 started after the formation of the horse shoe structure (ca 100.000 years ago) and continues to the present day. During this stage, the horseshoe shaped structure has been filled with andesitic domes and pyroclastic material. On the flanks some parasitic Pelean domes have also been formed at this time. These domes have aprons of unconsolidated block and ash flow deposits and dome flows (Roobol and Smith, 2004).

Since the European settlement on Saba in 1640 there has been no eruptive activity on the island. There are indications that the last eruption of Saba probably took place just prior to European settlement. Hot springs are at the moment the only volcanic activity observed on Saba. There are three hot springs known at sea level located at Well bay, between Ladder Bay and Tent Bay (last temperature measurement in 1997, 62°C) and one opposite of Green Island (last temperature measurement in 1998, 79°C) (Roobol and Smith, 2004). There is also heat escaping from a sulfur mine and divers found geothermal heat escape on the seafloor near Green Island. In total, six locations of heat escape are discovered which occur in two clusters of three. These clusters are located on opposite sides of the island which outline a northeast-southwest direction. This direction may mark a fault through the submarine banks beneath Saba. This possible fault may also control the

location of the main vent on Saba. Other indications supporting this fault are the orientation of the horseshoe shaped sector collapse scar and epicenters of earthquakes. The geothermal evidence suggests that there are still hot areas beneath Saba. For this reason the volcano must be classified as dormant instead of extinct (Roobol and Smith, 2004).

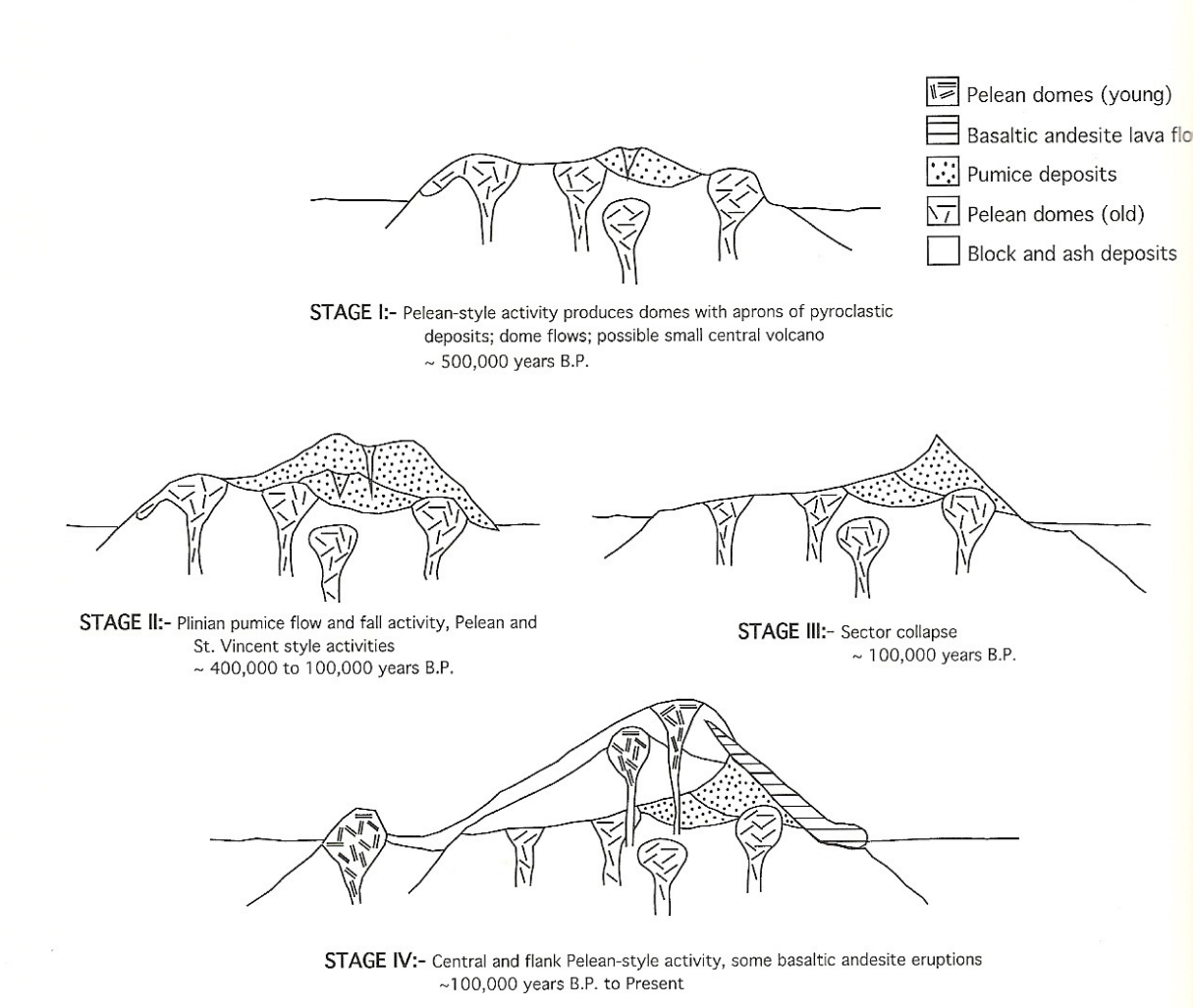

Figure 6: The four stages of structural evolution of Saba. (Roobol and Smith, 2004)

Chapter 3: Materials and Methods

3.1 Introduction

During the field campaign in June 2014 samples were collected for this project. Samples were collected from 56 different locations of the island for geochemical analysis (see Figure 7). Some parts of the island have a better sample coverage than other parts of the island (figure 7). This is because the island has a very dense forest at higher altitudes and has some very steep slopes along the coast, these conditions made it impossible to cover the whole island. Therefore most samples are taken along trails and coastal exposures. As also stated in the previous chapter, most of the sampled rocks are part of the stage 4 andesitic domes. Care was taken to sample both the mafic enclaves and host rocks.

All of the samples have been analyzed by XRF for major and trace- elements. A selection of 8 samples was also analyzed for trace elements by ICP-MS and isotope measurement by TIMS (Sr, Nd, Pb) and MC-ICPMS (Hf). Furthermore, a total of 10 samples were selected for trace element and isotope analysis of plagioclase separates.

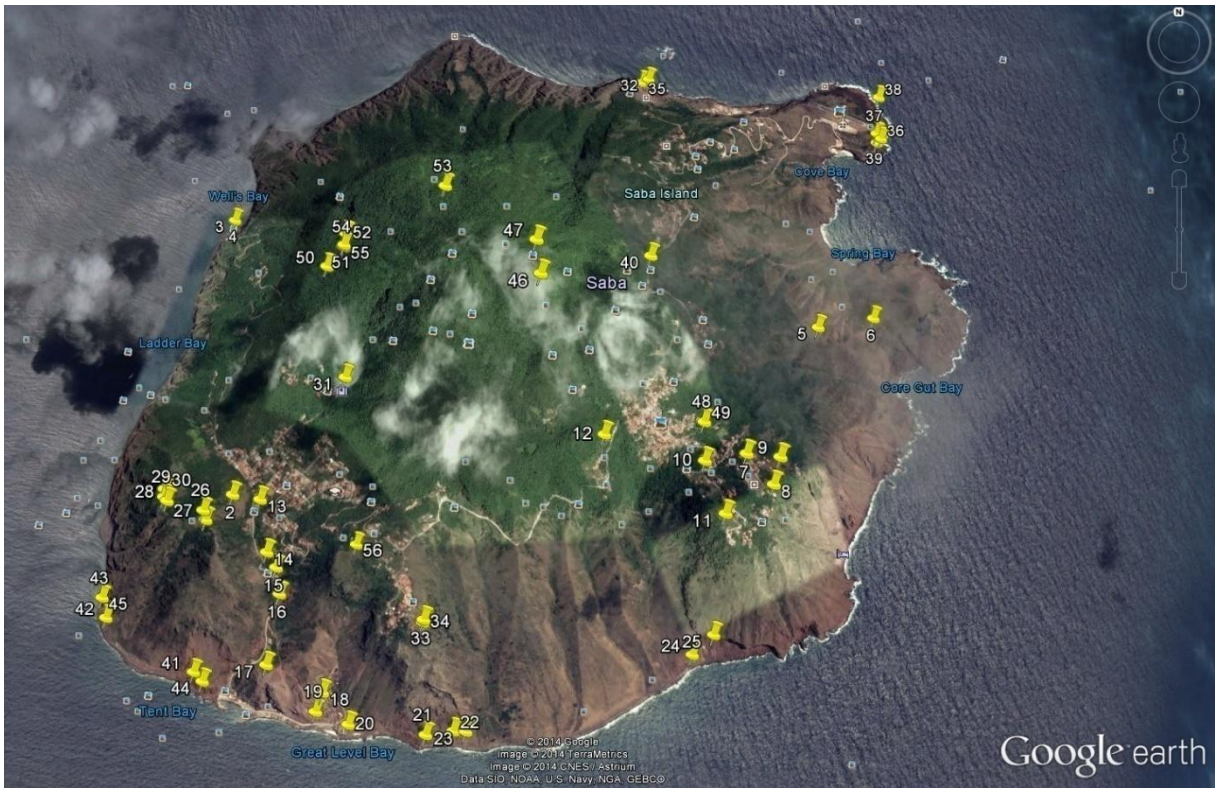

Figure 7: Map of Saba with sample locations

3.2 Powdering

The whole rock samples were processed to powders in the Mineral Separation Laboratory at the VU Amsterdam. First the samples were cut into blocks with an average size of ~4x5x3 cm using a diamond blade saw. Weathered pars were removed, and the blocks were ultrasonically cleaned in

deionized water for 15 minutes and dried at 50 C. Two or three blocks of each sample were crushed by a steel jawcrusher which reduced the sample to <1 cm chips. Subsequently, the chips were powdered in an shatter box for 1 minute and finally in an agate planetary ball mill for 60 minutes to a grain size of <2µm. The jawcrusher was cleaned after every sample with a steel brush, tissues with ethanol and compressed air. The agate parts were also cleaned after every sample with quartz sand and demineralised water. Ethanol and an hairdryer were used to dry the agate parts quickly.

3.3 Beats and Pellets

Fused glass beads and pressed powder pellets were prepared for the XRF analysis,. Beads are used to measure major element concentrations and pellets are used to measure trace element concentrations. To prepare the pellets and beats, first a rough 15 g of whole rock powder was dried at 120 C in a stove overnight. Afterwards the powder was stored in a desiccator to cool down.

Bead preparation doesn't only require a dry powder, but also the removal of volatiles such as water, sulfur and carbon. Therefore approximately 1,5 g of dried sample powder was stored in porcelain cups in an oven at 1000°C for 1 hour. The samples were weighed carefully on a 4 decimal balance before and after ignition. The change in mass represents the loss of ignition (LOI) which gives the wt.% of volatiles in the sample. After LOI determination, 1.000 g of sample powder was mixed in a mixing machine with 4.000 g of Spectroflux 110. This flux lowers the melting temperature of the sample. Subsequently, the sample was loaded in a platinum crucible and heated to ~1200°C in a Philips PerlX3 machine. Casting of the sample was done in a 30mm platinum casting dish. It is possible that the bead breaks during cooling, in this case the process was repeated using the broken bead. After every sample, the platinum dishes were cleaned in an ultrasonic bath with 40% citric acid.

For the pellets, 4.500 g sample powder was mixed in a mixing machine with 1/10 (0.450 g) of EMU 120 FD which is an organic binder. Subsequently, the mixture was put into a 30mm aluminum cup and loaded in the SpexCeripreppress model 3624. In this press the pressure was brought to 20 tons for at least 30 seconds, after which the pressure was released carefully. Every finished pellet was blown off with compressed air to remove minor flakes which could potentially damage the XRF.

3.4 Plagioclase separation

Plagioclase crystals of 10 samples were selected for ICP-MS analyses and Sr and Pb isotope analyses. The whole rock samples first went through a steel jawcrusher after which the separation process could start. To separate the plagioclase crystals from the matrix the first step involved separation with heavy liquids. This technique makes use of density differences between minerals and a dense liquid. Minerals in the liquid will either float (when less dense then the liquid) or sink (when denser then the liquid). The heavy liquid which is used at the VU is diiodomethene (CH_2I_2) which has a density of 3.34g/cm³. This liquid can be mixed with dichlorobenzene ($C_6H_4Cl_2$) to make any desired density. Plagioclase has a density between 2.62 g/cm³and 2.76 g/cm³. Therefore we used heavy liquids of 2.62 g/cm³ to separate plagioclase from less dense minerals and 2.76g/cm³ to separate

plagioclase from denser minerals. To speed up the separation, it is performed in a liquid overflow centrifuge which can reach a much higher gravitational acceleration (IJlst, 1976). The remaining material went through a Frantz isodynamic separator which separates the magnetic fraction from the non-magnetic fraction. Plagioclase is a non magnetic mineral. The magmatic separation started with I=50 mA, in each next step the power was doubled until the maximum power of 2 A was reached. Finally, 15-30 mg plagioclase of each sample were hand picked out of the remaining material which consisted mainly of quartz and plagioclase. Care was taken to select inclusion free plagioclases.

3.5 Cleanlab procedures

3.5.1 Cleaning beakers

Before starting sample dissolution and element separation procedures all lab ware must be cleaned carefully to ensure low blank levels for all elements of interest. This includes pipette tips, centrifuge tubes, PFA vessels and PFTE bombs. The pipette tips were cleaned in 500 ml 6-7 M Quartz Distilled (QD) HCl for 3 days and subsequently rinsed 5 times with milli-Q water. Centrifuge tubes were filled with 6-7 M HCl for 3 days and rinsed 4 times with milli-Q water. All acids used are DT distilled. Milli-Q water has a resistance of $10^{18}\Omega$. The following steps were carried out for cleaning PFA vessels and teflon bombs:

1. Cleaning with cotton wool and ethanol to remove organic compounds and old tags.
2. Boiling in pa quality HNO_3 for 1,5 hours, rinse 3 times with demineralised water.
3. Boiling in pa quality HCl for 1,5 hours, rinse 3 times with demineralised water.
4. Cleaning with double distilled 6-7M QD HCl for approximately 2-3 days, rinse 4 times with milli-Q water.
5. Cleaning with 30 droplets concentrated Teflon Distilled (TD) HNO_3 and 10 droplets concentrated TD hydrofluoric acid (HF) for approximately 2-3 days, rinse 4 times with milli-Q water.
6. The PFA vessels used for Pb were also cleaned with 0,7 M TD HBr for 2-3 days and rinsed afterwards 4 times with milli-Q water.

3.5.2 Sample dissolution

A completely dissolved sample is needed for ICP-MS analysis and Sr, Nd, Pb element separation. Since zircon could be an accessory mineral in the Saba volcanics, Parr-bombs were used (Mahlen et al., 2008). Besides the 8 whole rock samples also one USGS international standard (AGV-2) and one blank were included.

Whole rock powder (65-75 mg) was weighed for all samples and standards. This was put in the Teflon bombs together with 2,5 ml TD concentrated HF and 20 droplets TD HNO_3. The Teflon bombs were sealed and mounted in steel-jacketed Parr-bombs. These bombs were placed in an oven at 200°C for five days. Subsequently, the samples were transferred into clean 30 ml PFA beakers in 6-7M QD HCl. The samples were dried down on a 120°C hot plate and nitrated twice with 15-20 drops concentrated TD HNO_3. The HNO_3 breaks insoluble chloride- and fluoride salts down. Finally, the samples were taken up in 5 ml 3M TD HNO_3.

For ICP-MS analysis an aliquot of~0,15 ml was taken from the total solution of ~5 ml. This aliquot was diluted ~5000 times with 5% HNO_3 and stored in a 10 ml centrifuge tube. Every step was weighted carefully to be able to calculate the exact dilution factor. Before analysis, samples were homogenized and centrifuged.

3.5.3 Sr extraction

The element strontium can be separated from other elements using Eichrom's Sr Resin. This resin is an extraction chromatographic material in which the extracting system is 1.0M 4,4(5')-di-t-butylcyclohexano 18-crown-6 (crown ether) in 1-octanol[1]. The resin was loaded into 1 ml columns with a filter made of quartzwool. Subsequently, the columns were rinsed with three times 1 reservoir volume of 3M TD HNO_3 and 1 reservoir volume water. In the next step the columns were conditioned with half a reservoir volume 3M HNO_3. Before loading, the samples were ultra-sonificated for 1 hour and centrifuged for 5 minutes at 4000 rpm. An aliquot corresponding to 500 ng strontium was loaded onto the columns. The other elements were rinsed off with 2 ml 3M HNO_3. 1 ml milli-Q water was used for elution of the Sr-fraction. One drop of 0,5% phosphoric acid (H_3PO_4) was added to the Sr-fractions before they were dried down on a hot plate. H_3PO_4 facilitates in the loading of the samples for TIMS analysis and does not increase the blank values. An 84-Sr spike (code 20130705) was added to the blank. Finally, the samples were dried down on a hot plate at 120°C.

3.5.4 Nd extraction

To separate neodymium from the matrix two column extractions are required. In the first column procedure (TRU-spec) the light to middle rare earth elements (REE) are separated from the matrix. In the second column procedure (LN-spec) the Nd is separated from other REE elements.

The TRU-spec resin is an extraction chromatographic material in which the extractant system is octylphenyl-N, N-di-isobutyl carbamoylphosphine oxide (CMPO) dissolved in tri-n-butyl phosphate (TBP)[2].This resin was loaded into 0,15 ml quartz columns with a polyethylene filter. The columns were rinsed twice with 1 ml 2M TD HNO_3 and 1 ml milli-Q water. Subsequently, the columns were conditioned with 1 ml 2M TD HNO_3. Before loading the samples, the samples were ultra-sonificated for half an hour, homogenized and centrifuged for 5 minutes at 4000 rpm. Subsequently the sample was loaded on to the columns in 3M TD HNO_3. The other elements were removed with 3.6 ml 2M TD HNO_3. 1.5 ml milli-Q water was used for elution of the light to middle REE. The REE-fraction was dried down on a hotplate at 120°C, nitrated with 2 drops of concentrated TD HNO_3 and dissolved again in 1 ml 0,165 M TD HCL.

The Ln resin is an extraction chromatographic material in which the extractant system is di(2-ethylhexyl) orthophosphoric acid (HDEHP)[3]. The Ln-column Nd extraction procedure takes two days. 1 reservoir volume is approximately 3.8 ml. At the first day the columns are pre-cleaned by the following steps:

[1] http://www.eichrom.com/products/info/sr_resin.aspx
[2] http://www.eichrom.com/products/info/tru_resin.aspx
[3] http://www.eichrom.com/eichrom/products/info/ln_resin.aspx

1. Washed with 1 reservoir volume 6-7 M QD HCl.
2. Washed with 1 reservoir volume 2 M TD HF.
3. Washed with 1 reservoir volume Milli-Q water.
4. Washed with 1 reservoir volume 6-7 M QD HCl.
5. Washed with 1 ml 0.165 M TD HCl and stored in 10 ml centrifuge tubes overnight.

The next day the columns were first conditioned with 1 reservoir volume 0.165 M TD HCl. Before loading, the samples were heated to 70-80°C for a day, ultra-sonificated for 30 minutes and centrifuged at 12000rpm for 4 minutes. Subsequently, the samples were loaded onto the columns. The other elements were eluted with 9.5 ml 0.165 M HCl. The Nd fraction was eluted with 4 ml 0.3 M HCL. An 150-Nd spike (code 20110303) was added to the blank. One drop of 0,5% phosphoric acid (H_3PO_4) was added to the Nd-fractions before they were dried down on a hot plate at 120°C.

3.5.5 Pb extraction

The element lead can be separated from other elements using AG-X8 Pb Resin. This resin was already loaded into 1 ml columns and can be used multiple times. Because the plagioclase samples had very low Pb concentrations, new columns were made for these samples. Subsequently, the columns were pre-cleaned with 0.5 ml 0.7 M TD HBr. Before loading, the samples were ultra-sonificated for 0.5 hour and centrifuged for 5 minutes at 4000 rpm. After loading of the samples, the columns were rinsed two times with 0.5 ml 0.7 M TD HBr and once with 0.1 ml 3 M TD HCl. The Pb fraction was eluted with 0.5 ml 6 M QD HCl. An 208-Pb spike (code 9211290) was added to the blank before the samples were dried down on a hot plate at 120°C.

3.6 Measuring techniques

3.6.1 XRF analysis

Major, trace and limited rare-earth elements are measured using the PanalyticalAxiosMax Fluorescence (XRF) spectrometer. Major elements (Fe, Mn, Ti, Ca, K, P, Si, Al, Mg, Na, Ba) were measured using glass beads. These data are expressed as weight percentage of the oxides. Trace elements and limited REE (La, Ce, Pr, Nd, Sm, Ga, Zn, W, Ta, Cu, Hf, Er, Ni, Yb, Dy, V, Cr, Co, Ba, Sc, Er, Hf, Mo, Nb, Y, Zr, Sr, U, Rb, Th, Pb and K) were measured using pressed powder pellets. For the trace element measurements there are four different programs called; Metals, Reehex, Spel and VCrCoBaSc. During each program, four USGS reference materials are also measured to check the precision and accuracy of the measurements. These reference materials are AGV-1, GSP-1, BHVO-2 and BCR-2 for the major element program and AGV-2, GSP-2, BHVO-2 and BCR-2 for the trace element programs. Table 1 and Table 2 show reference values and the measured data for the used standards. Reference values were found on http://georem.mpch-mainz.gwdg.de/sample_query.asp.

	GSP-1						AGV-1					
	average	SD	n	CV	accuracy	reference	average	SD	n	CV	accuracy	reference
Fe2O3	4,29	0,00	3	0,07	0,03	4,29	6,91	0,01	3	0,17	2,04	6,77
MnO	0,04	0,00	3	0,00	2,50	0,04	0,10	0,00	3	0	6,52	0,092
TiO2	0,66	0,00	3	0,00	1,23	0,65	1,07	0,00	3	0,14	1,46	1,05
CaO	2,01	0,00	3	0,09	2,80	2,07	5,03	0,01	3	0,15	1,92	4,94
K2O	5,57	0,00	3	0,07	1,05	5,51	3,03	0,01	3	0,18	3,69	2,92
P2O5	0,28	0,00	3	0,20	0,60	0,28	0,51	0,00	3	0,2	1,20	0,5
SiO2	67,93	0,06	3	0,09	1,05	67,22	60,57	0,09	3	0,15	2,94	58,84
Al2O3	15,15	0,01	3	0,07	0,35	15,1	17,46	0,02	3	0,12	1,82	17,15
MgO	0,97	0,00	3	0,31	0,63	0,96	1,54	0,00	3	0,16	0,76	1,53
Na2O	2,79	0,00	3	0,07	0,26	2,8	4,78	0,00	3	0,06	12,14	4,26
BaO	0,15	0,00	3	0,00	0,68	0,146	0,14	0,00	3	0,84	0,24	0,137
	GSP-2						AGV-2					
	average	SD	n	CV	accuracy	reference	average	SD	n	CV	accuracy	reference
La	171,08	9,16	3	5,356	4,95	180	39,98	1,02	3	2,56	5,48	37,9
Ce	420,15	27,62	3	6,573	2,48	410	68,62	2,34	3	3,42	0,02	68,6
Pr	39,68	2,88	3	7,25	22,20	51	9,00	0,40	3	4,43	14,84	7,84
Nd	175,04	3,13	3	1,788			25,67	1,68	3	6,54	15,83	30,5
Sm	27,72	0,23	3	0,812			4,87	0,55	3	11,3	11,29	5,49
Ga	22,30	0,01	2	0,063	1,36	22	20,87	0,11	2	0,51	4,33	20
Zn	117,75	0,33	2	0,282	1,88	120	92,05	0,16	2	0,18	7,03	86
Cu	40,93	0,25	2	0,605	4,83	43	53,20	0,16	2	0,31	0,37	53
Hf	12,86	0,32	2	2,475	8,18	14	6,49	0,26	2	4,03	29,70	5
Er	3,23	0,47	2	14,45	46,82	2,2	2,80	0,16	2	5,56	54,70	1,81
Ni	18,22	0,09	2	0,505	7,15	17	18,88	0,25	2	1,35	5,60	20
Yb	5,35	0,18	2	3,436			5,21	0,05	2	0,95	221,30	1,62
Dy	3,26	0,74	2	22,81	46,64	6,1	3,01	0,12	2	4	13,40	3,47
V	53,72	1,14	3	2,121	3,31	52	121,16	0,75	3	0,62	0,69	122
Cr	20,48	0,25	3	1,222	2,38	20	15,90	0,13	3	0,85	0,62	16
Co	6,49	0,28	3	4,323	11,10	7,3	16,86	0,15	3	0,87	5,40	16
Ba	1299,28	2,19	3	0,168	3,04	1340	1118,07	2,84	3	0,25	1,06	1130
Sc	7,29	0,66	3	9,089	15,77	6,3	15,54	0,32	3	2,03	19,56	13
Hf	10,74	0,47	3	4,411	23,26	14	5,72	0,67	3	11,7	14,47	5
Mo	2,62	0,10	3	3,761	24,92	2,1	2,13	0,10	3	4,57		
Nb	24,96	0,07	3	0,261	7,57	27	13,13	0,03	3	0,2	9,45	14,5
Y	22,57	0,07	3	0,302	16,42	27	18,47	0,15	3	0,82	2,77	19
Zr	502,74	0,15	3	0,029	8,59	550	220,54	0,05	3	0,02	4,11	230
Sr	229,61	0,22	3	0,094	4,33	240	631,19	0,34	3	0,05	4,51	661
U	2,60	0,23	3	8,762	8,47	2,4	1,30	0,06	3	4,62	30,11	1,86
Rb	241,51	0,21	3	0,086	1,42	245	66,45	0,06	3	0,09	0,23	66,3
Th	111,21	0,28	3	0,255	5,91	105	6,31	0,16	3	2,48	3,44	6,1
Pb	40,88	0,30	3	0,735	2,67	42	12,52	0,14	3	1,13	5,15	13,2

Table 1: Measured and reference values and the coefficient of variation (CV) and accuracy for GSP-1, GSP-2, AGV-1 and AGV-2.

	BHVO-2						BCR-2					
	average	SD	n	CV	accuracy	reference	average	SD	n	CV	accuracy	reference
Fe2O3	12,35	0,01	3	0,06	0,98	12,23	13,85	0,01	3	0,06	0,39	13,80
MnO	0,17	0,00	3	0	1,81	0,17	0,20	0,00	3	0,29	1,19	0,20
TiO2	2,73	0,00	3	0,04	0,48	2,72	2,26	0,00	3	0,07	0,01	2,26
CaO	11,36	0,01	3	0,05	0,25	11,34	7,13	0,00	3	0,05	0,20	7,12
K2O	0,52	0,00	3	0,11	1,62	0,51	1,80	0,00	3	0,12	0,41	1,79
P2O5	0,27	0,00	3	0,22	0,50	0,27	0,35	0,00	3	0,16	0,76	0,35
SiO2	49,76	0,05	3	0,1	0,29	49,62	54,46	0,03	3	0,05	0,66	54,10
Al2O3	13,49	0,01	3	0,09	0,50	13,42	13,55	0,01	3	0,11	0,36	13,50
MgO	7,16	0,00	3	0,05	0,41	7,19	3,60	0,00	3	0,07	0,17	3,59
Na2O	2,20	0,00	3	0,1	0,12	2,21	3,15	0,00	3	0,1	0,25	3,16
BaO	0,01	0,00	3	4,03	1,15	0,01	0,08	0,00	3	0	1,32	0,08
La	11,95	2,61	3	21,8	20,36	15	22,32	0,49	3	2,2	10,72	25
Ce	42,59	1,11	3	2,61	12,09	38	57,15	0,71	3	1,25	7,84	53
Pr	5,53	0,46	3	8,24	3,30	5,35	7,66	0,19	3	2,49	12,60	6,8
Nd	27,84	2,14	3	7,67	11,35	25	28,54	1,53	3	5,36	1,94	28
Sm	6,04	0,29	3	4,82	2,53	6,2	6,28	0,04	3	0,64	6,27	6,7
Ga	22,41	0,03	2	0,13	3,27	21,7	22,73	0,01	2	0,06	1,17	23
Zn	114,39	0,11	2	0,09	11,05	103	132,56	0,04	2	0,03	4,37	127
Cu	134,15	0,05	2	0,04	5,63	127	19,44	0,33	2	1,71	2,29	19
Hf	5,23	0,07	2	1,35	27,56	4,1	6,12	0,13	2	2,08	27,50	4,8
Er	3,08	0,16	2	5,05	21,26	2,54	4,34	0,76	2	17,5	18,44	3,66
Ni	131,05	0,34	2	0,26	10,13	119	10,10	0,47	2	4,69	43,92	18
Yb	5,14	0,37	2	7,15	157,00	2	6,80	1,13	2	16,6	94,29	3,5
Dy	9,71	0,45	2	4,66	82,86	5,31	10,94	1,53	2	14	70,67	6,41
V	313,49	0,66	3	0,21	1,11	317	405,85	0,84	3	0,21	2,44	416
Cr	292,70	0,47	3	0,16	4,54	280	19,19	0,28	3	1,46	6,59	18
Co	43,65	0,13	3	0,29	2,99	45	37,73	0,36	3	0,95	1,97	37
Ba	124,93	1,66	3	1,33	4,63	131	690,45	2,00	3	0,29	1,99	677
Sc	34,60	0,14	3	0,4	8,12	32	30,44	0,44	3	1,46	7,77	33
Hf	5,87	0,80	3	13,6	34,63	4,36	6,50	0,18	3	2,79	32,59	4,9
Mo	3,31	0,08	3	2,36	17,25	4	221,20	0,22	3	0,1	10,81	248
Nb	17,59	0,12	3	0,66	2,26	18	11,63	0,06	3	0,5	7,67	12,6
Y	27,78	0,11	3	0,4	6,85	26	38,65	0,09	3	0,23	4,45	37
Zr	161,91	0,40	3	0,25	5,86	172	177,63	0,11	3	0,06	5,51	188
Sr	383,53	0,56	3	0,15	1,41	389	334,58	0,40	3	0,12	3,30	346
U	0,19	0,17	3	89,5	52,85	0,403	1,58	0,17	3	11	6,51	1,69
Rb	8,78	0,08	3	0,89	10,44	9,8	47,69	0,05	3	0,1	0,65	48
Th	1,17	0,08	3	6,87	2,78	1,2	6,47	0,31	3	4,77		6,2
Pb	0,52	0,23	3	43,6			9,14	0,24	3	2,65	16,91	11

Table 2: Measured and reference values and the coefficient of variation (CV) and accuracy forBHVO-2 and BCR-2.

3.6.2 ICP-MS analyses

Trace element concentrations of 8 whole rock and 10 plagioclase samples were measured at the VU University Amsterdam using a quadrupole Thermo X-Series II inductively coupled plasma mass spectrometer (ICP-MS).The ICP-MS measurement protocol used a method modified after Eggins et al., (1997). The ICP-MS is calibrated with a BHVO-2 international standard which is measured at the start of each sample series. The BHVO-2 is also used for drift correction.

	AGV-2 measured	reference	±	Accuracy
Li	11,40	11,00	1,00	3,522
Be	2,21	2,30	0,40	3,980
Sc	12,33	13,00	1,00	5,395
V	116,42	120,00	5,00	3,076
Cr	21,56	17,00	1,00	21,132
Co	15,37	16,00	1,00	4,111
Ni	16,69	19,00	1,00	13,825
Cu	49,33	53,00	4,00	7,441
Zn	78,78	86,00	8,00	9,159
Ga	19,56	20,00	1,00	2,237
Rb	68,44	66,30	0,50	3,127
Sr	638,43	661,00	6,00	3,535
Y	20,43	19,00	2,00	6,978
Zr	238,62	230,00	4,00	3,613
Nb	14,66	14,50	0,80	1,095
Cs	0,56	1,16	0,08	106,596
Ba	1118,88	1140,00	32,00	1,888
La	37,41	37,90	0,04	1,321
Ce	69,68	68,60	0,50	1,554
Pr	7,93	7,84	0,31	1,160
Nd	29,92	30,50	0,10	1,938
Sm	5,38	5,49	0,03	2,109
Eu	1,55	1,53	0,02	1,546
Tb	0,62	0,64	0,01	3,407
Gd	4,43	4,52	0,05	2,030
Dy	3,47	3,47	0,03	0,121
Ho	0,64	0,65	0,03	1,305
Er	1,77	1,81	0,02	2,224
Tm	0,26	0,26	0,01	0,984
Yb	1,56	1,62	0,02	3,707
Lu	0,24	0,25	0,00	4,255
Hf	4,88	5,00	0,10	2,493
Ta	0,87	0,87	0,08	0,371
Pb	9,02	13,20	0,50	46,418
Th	6,19	6,10	0,20	1,456
U	1,83	1,86	0,09	1,620

Every sample was diluted ~5000 times with 5% HNO_3 in a 10 ml centrifuge tube. By weighing after every step, exact dilution factors were calculated. The samples were homogenized and centrifuged for 10 minutes at 4000 rpm before analysis with ICP-MS.

One USGS international standard (AGV-2) underwent the same procedure as the other samples and was also analyzed by ICP-MS. Table 3 shows the measured values compared with the reference values of AGV-2.

Most of the data are within the measurement uncertainty of the reference value. Errors in the measurement can be noted for the values of Cr, Pb and Cs. Fortunately, the values of Cr and Cs are not used in this research. In section 3.6.4 the XRF and ICP-MS data of Pb are compared to determine whether XRF or ICP-MS results should be used for this element. With other elements, the accuracy is better than 5%.

Table 3: Measured values and reference values of AGV-2 for ICPMS analyses (http://crustal.usgs.gov/geochemical_reference_standards/pdfs/andesite2.pdf)

3.6.3 TIMS

The Sr, Nd and Pb isotopes were measured using a TritonPlus Thermal Ionization Mass Spectrometer (TIMS). The Sr fractions were loaded onto pre-cleaned (boiled for half an hour in distillated water and demineralized water) and outgassed single rhenium filaments. For each sample the fraction was re-dissolved in 2 µl 10% HNO_3. Subsequently, each fraction was loaded on the filaments together with 2 µl of a $TaCl_5$ activator. The activator serves to facilitate efficient and stable evaporation of strontium in the ion source. Nd fractions were loaded onto pre-cleaned and outgassed double rhenium filaments. Pb fractions were loaded onto pre-cleaned and outgassed single zone refined rhenium filaments. For every Pb sample two fractions were loaded where a $^{207}Pb/^{204}Pb$ enriched spike was added to one of them, this is called the 'double spike method'. Nd and Pb samples were run in a static program (Sr in a dynamic program) and were heated to approximately 1350°C. For the Pb samples heating was fast at the start and slowly at the end. Data were acquired in 5 blocks of 20 scans. Unfortunately the Pb measurements failed.

To access the precision and reproducibility of the sample series, the SRM 987 strontium standard was measured at least once a day. The blank and USGS samples (AGV-2) were treated the same way as the samples. To check whether the lab procedures had any effect on isotope compositions these samples were also analyzed. The measurement results are shown in table 4. SRM 987 has a reference value of 0,710248, this value lies within the errors of the measured values (0.710248 +/- 0,00000228 (2sd). AGV-2 reference values are obtained from http://georem.mpch-mainz.gwdg.de and show $^{87}Sr/^{86}Sr$ range from 0,703931 to 0,704079, $^{143}Nd/^{144}Nd$ ranges from 0.512755 to 0.512811.

Sample	$^{87}Sr/^{86}Sr$ ratio	Error (2se)	$^{143}Nd/^{144}Nd$ ratio	Error (2se)
SRM 987	0,710248	0,000008		
	0,710248	0,000007		
	0,710247	0,000008		
	0,710249	0,000006		
	0,71025	0,000008		
AGV-2	0,703973	0,000006	0,512783	0,000003
SB021B	0,703754	0,000008	0,51298	0,000003
SB054A	0,703765	0,000008	0,512936	0,000003
SB032D	0,704171	0,000008	0,51296	0,000003
SB006	0,703997	0,000007	0,51296	0,000003
SB024AII	0,703747	0,000009	0,512967	0,000003
SB008AII	0,70379	0,000007	0,512976	0,000003
SB016	0,703857	0,000008	0,512972	0,000003
SB024BII	0,703483	0,000007	0,512973	0,000003
Plagioclase samples				
SB054A	0,703719	0,000007		
SB039I	0,70374	0,000008		
SB012	0,70372	0,000008		
SB053B	0,703731	0,000007		
SB045	0,703733	0,000008		
SB038B	0,703745	0,000008		
SB016	0,703775	0,000008		
SB054B	0,703724	0,000007		
SB010	0,703725	0,000006		
SB025	0,70372	0,000008		

Table 4: Measured Sr and Nd ratios

3.6.4. XRF and ICP-MS comparison

Generally XRF results are more accurate then ICP-MS results for high element concentrations but this also depends on the element. ICP-MS is often the most accurate measurement technique for concentrations below 10ppm. For 8 whole rock samples, several trace elements which were measured on the XRF were also measured on the ICP-MS. Figure 8 shows a comparison between data obtained from the two different measurement methods. Systematically higher concentrations of the element niobium are measured in the ICP-MS measurement. Systematically lower concentrations of the element ytterbium were measured on the ICPMS. ICP-MS data are more accurate than XRF data for ytterbium.

Strontium, lead and cerium are scattered but do not have a consisted offset. XRF analyses of these elements are in good agreement with the reference values. Lanthanum shows a large scatter. Because La concentrations are low in the Saba samples, ICP-MS measurements are more accurate than XRF measurements. XRF analysis of zirconium and yttrium are in good agreement with ICP-MS data. For these elements XRF data will be used because they are more abundant.

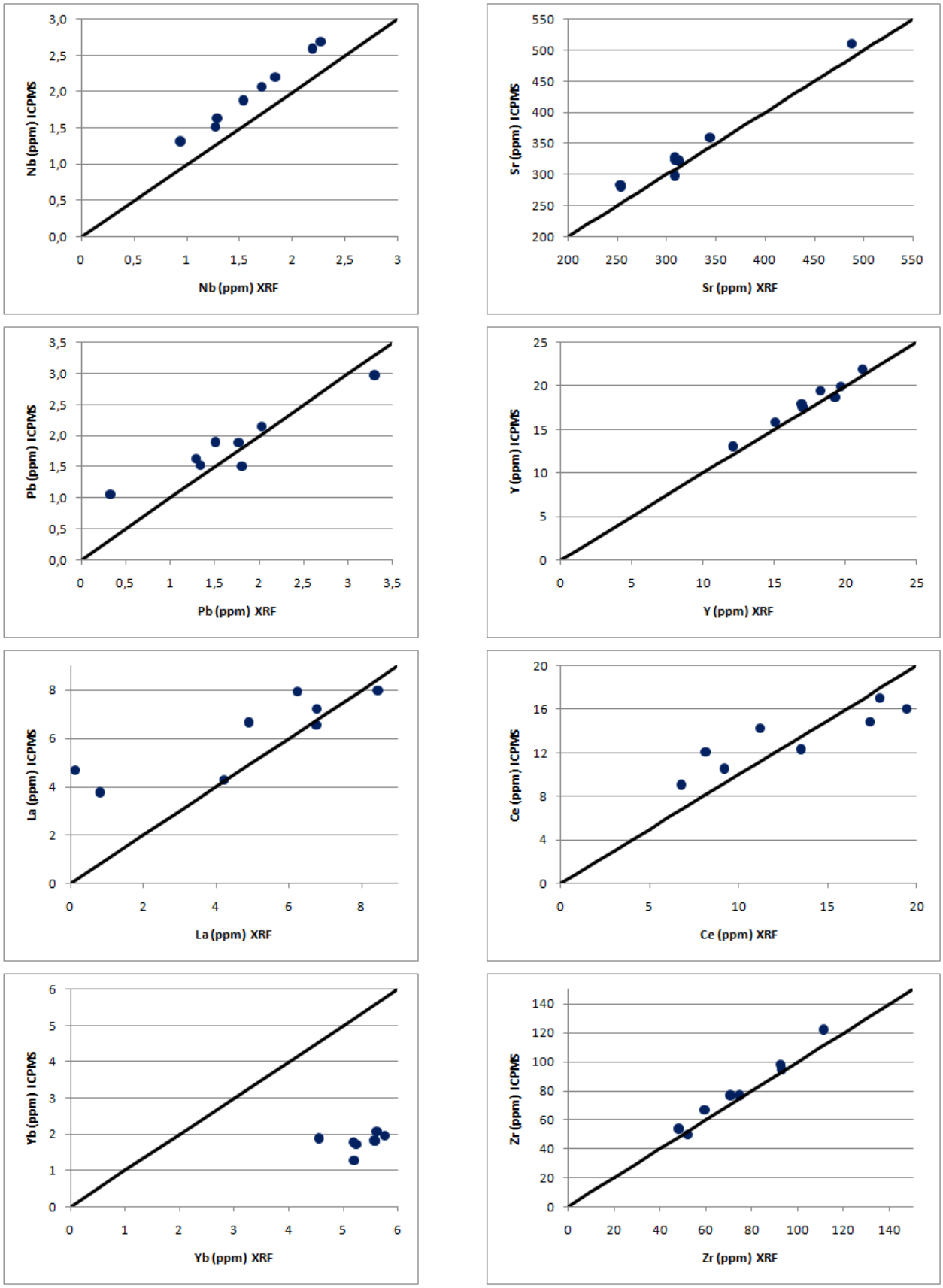

Figure 8: comparison of XRF and ICPMS results

Chapter 4: Results

4.1 Introduction

Our measured XRF data is subdivided into Saint Martin rocks, Saba hostrocks and Saba enclaves. Both the hostrocks and enclaves are subdivided into pre- and post-horseshoe structure based on the Roobol and Smith's geological map of Saba. The enclaves are also subdivided into porphyritic-, equigranular- and sedimentary enclaves, based on macroscopic determination. Each unit is indicated by its own symbol in the graphs. The classification of the volcanic samples of Saba and Saint Martin is based on a diagram comparing the total alkalis ($Na_2O + K_2O$) with silica ("TAS" after Le Bas et al. 1986. As shown in Figure 9, the Saba volcanics vary from basaltic (mostly enclaves) to andesitic (mostly hostrocks). The Saint Martin samples mainly consist of dacites and high SiO_2 andesites. Besides our own investigated samples, we also used previously published data from Roobol and Smith, 2004. This data is displayed as 'the gray cloud'.

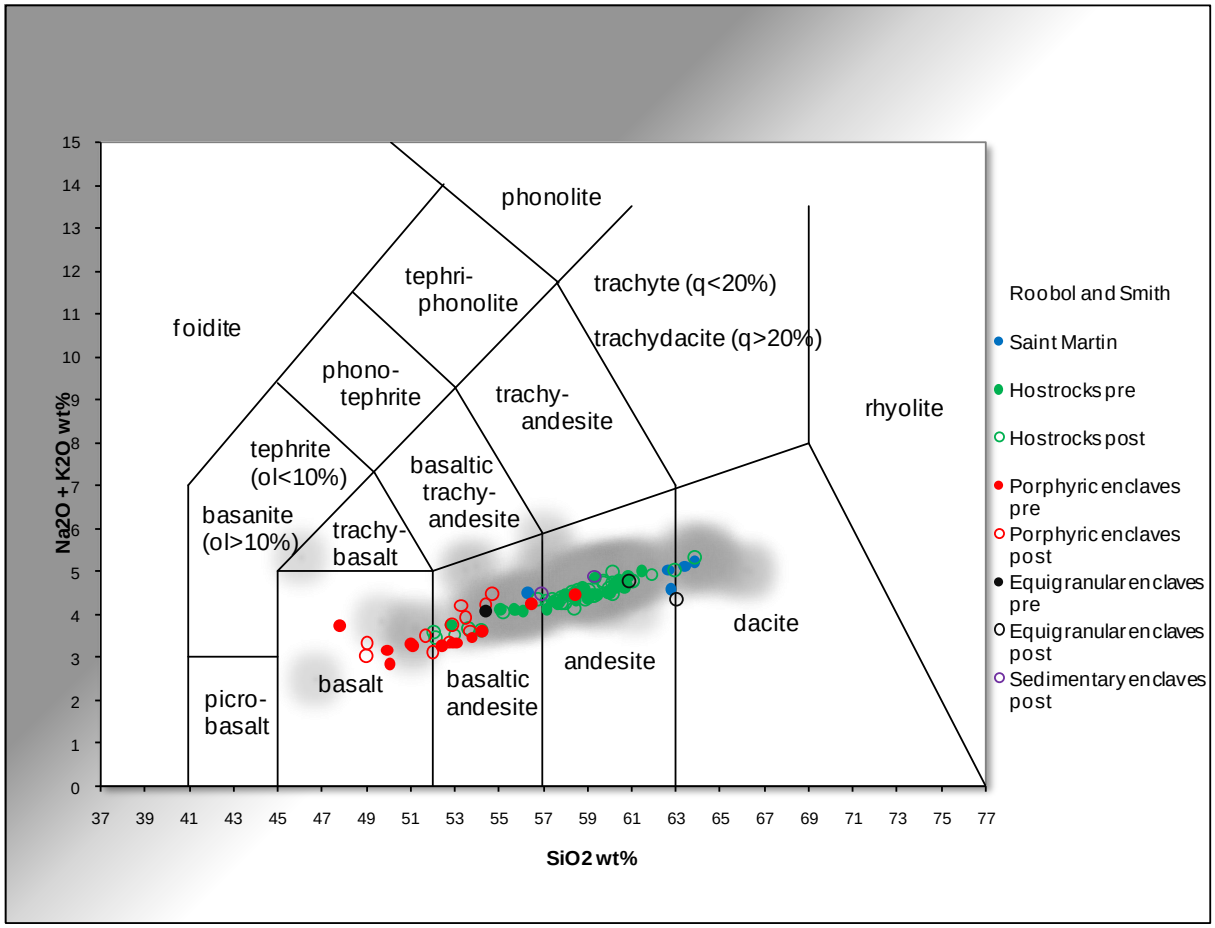

Figure 9: TAS diagram of Saba and Saint Martin samples

4.3 Field- and thin section observations

During the fieldwork a couple of important observations were made. The most important observation for this project is that nearly all the volcanic rocks on Saba show evidence for magma mixing like mingling and mafic enclaves as shown in Figure 10. Most rocks have phenocrysts of plagioclase and amphibole.

Figure 10: Mixing and mingling structures in magmatic rocks of Saba

Furthermore a temperature measurement on the hot spring opposite of Green Island was done. The measured temperature was 89°C which is an increase of 10°C since the last measurement in 1998 (Roobol and Smith, 2004). Also a landslide on the western side of the island was probably triggered by hydrothermal alteration of the rocks (photo on front page). On a slowly growing spot near Paris Hill, the vegetation suddenly died and the ground is turning black. These observations could be related to increasing magmatic activity below Saba and gasses which are forcing their way up.

In thin section most rocks consist mainly of plagioclase. Amphibole is also a very common phenocryst which is more abundant in the enclaves. Other observed minerals are clinopyroxene, olivine, quartz and opaque minerals. Especially the combination of quartz and olivine raises questions. At least three generations of plagioclase could be observed; altered large phenocrysts with sieve textures, stable large phenocrysts and smaller phenocrysts.

4.2 Harker variation diagrams

The Harker variation diagram is a simple x-y diagram, which plots wt.% silica on the x-axis against the other major oxides (Figure 11). SiO_2 increases steadily with magmatic differentiation, so the x-axis indicates the extent of differentiation. Normally, the magma with the lowest silica content is accepted as the parental magma. In case of Saba, the lowest silica content is found in the enclaves. The mafic enclaves likely entered the magma chamber later than the host rocks. Therefore in case of Saba the lowest silica contents cannot be seen as parental magma's. SiO_2 was also plotted against the minor/trace elements Sr, Pb, Ba, Nb, Y, Zr, Ce and Yb. The results are shown in Figure 11 and Figure 12. Error bars are shown in the upper right corner for both x and y values and are showing two standard deviations of the internal measurement differences. Errors in the major element diagrams are smaller than the symbol size and therefore not shown. Reference values can be found in Table 1,

Table 2 and Table 3. The observation that mixing processes beneath Saba are abundant also means that the Harker variation diagrams probably do not represent the fractional crystallization trend only.

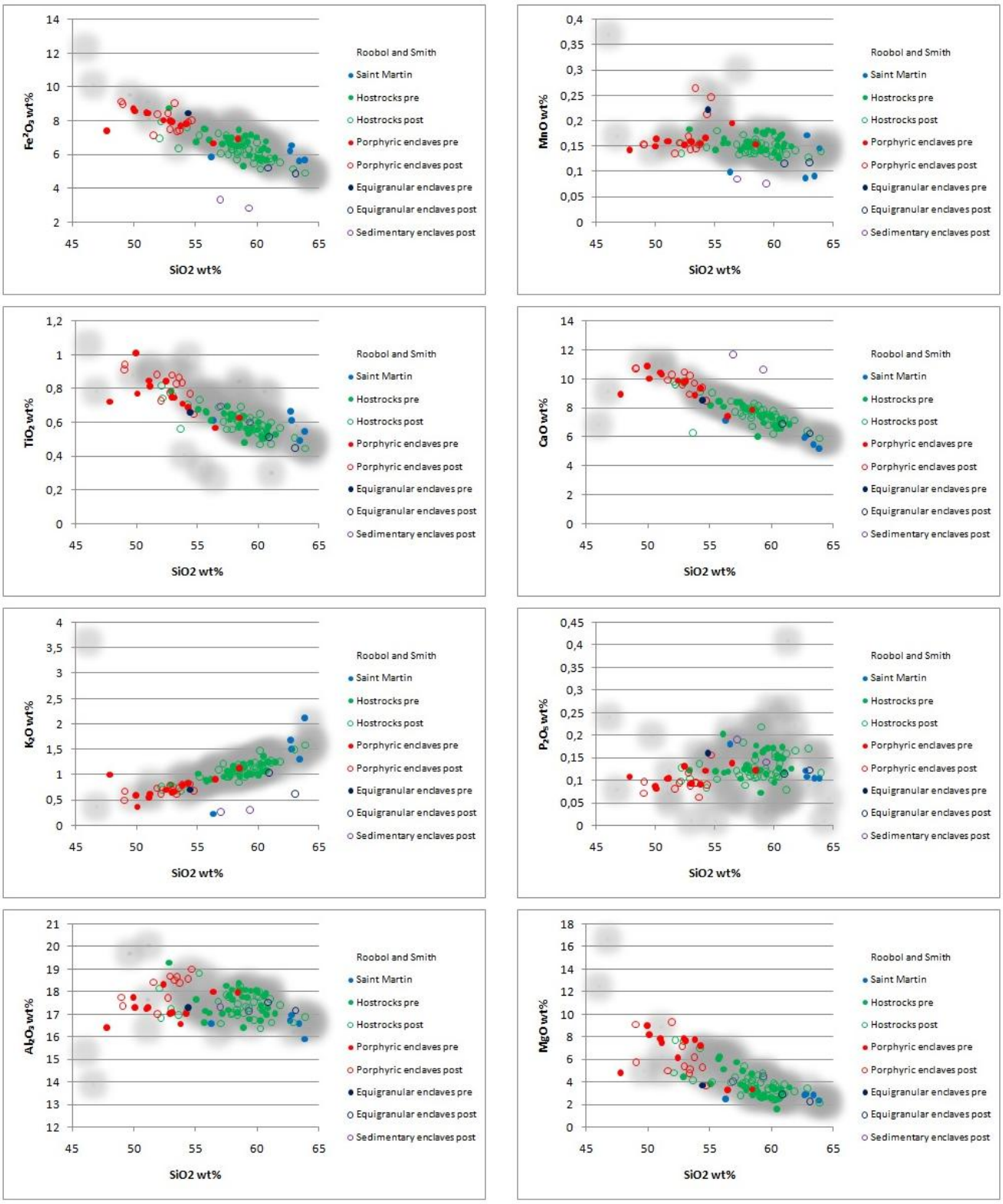

Figure 11: Variation diagrams of major elements against SiO_2

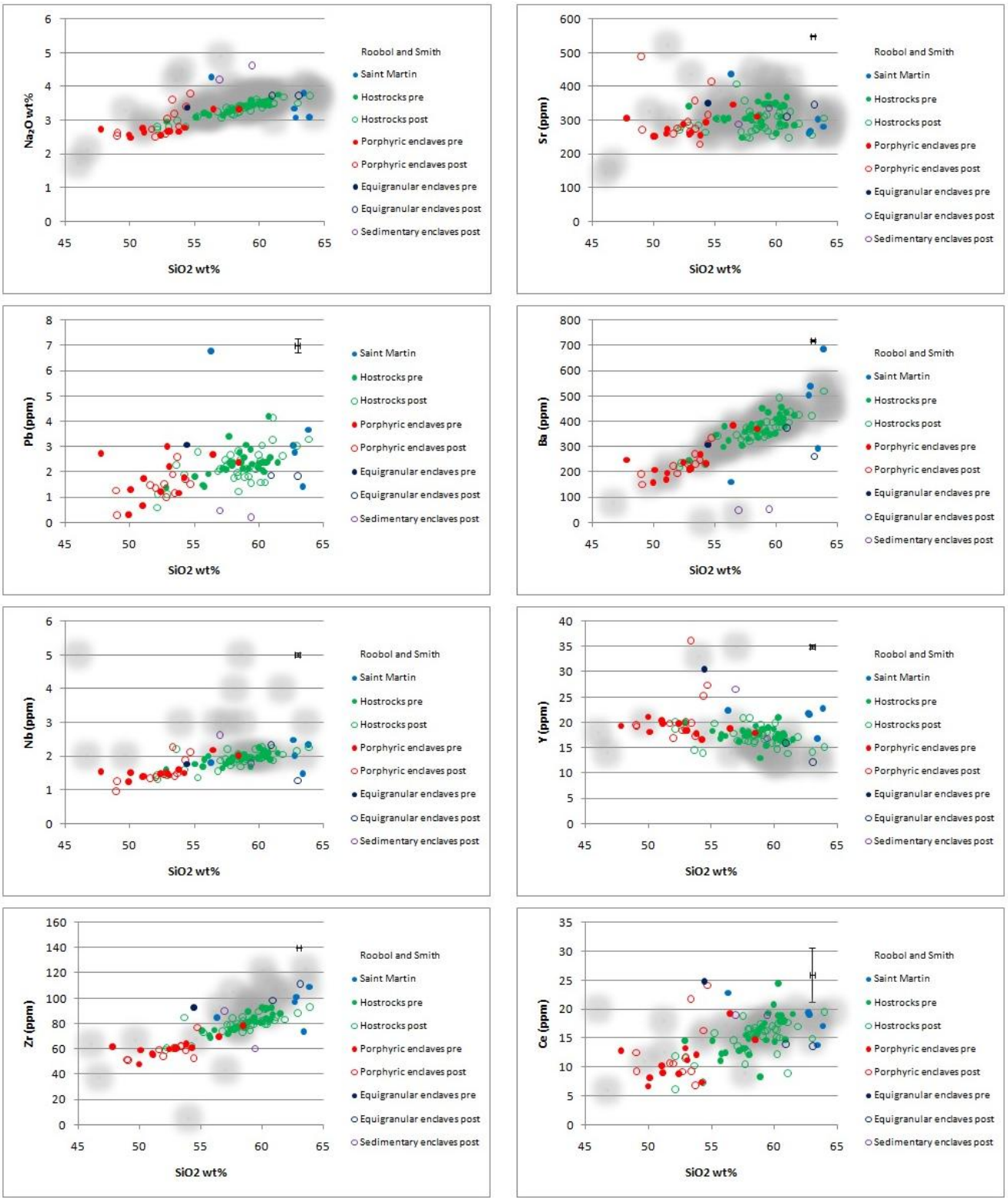

Figure 12: Variation diagrams of major and trace elements against SiO_2

The Harker variation diagrams show that the SiO_2 content in the rocks ranges from 47,5-64%. Pre horseshoe structure hostrocks show a larger variation in SiO_2 content (52-64%) than the post horseshoe structure hostrocks (53-61%). The porphyritic enclaves range mainly from 47,5-54% SiO_2 but there are a few exceptions with higher SiO_2 contents. Although there are only two samples of post horseshoe structure equigranular enclaves, these enclaves can be seen as an individual group because their SiO_2 contents are very high compared to the porphyritic enclaves. The pre horseshoe structure equigranular enclave overlap with the porphyritic enclaves. Fe^2O_3, TiO_2 and CaO show a smooth decreasing trend with increasing SiO_2. MgO also decreases with increasing SiO_2 but more variation in MgO content can be noticed especially in the post horseshoe structure porphyritic enclaves. MnO stays around 0,15 wt% when SiO_2 content increases. Post horseshoe structure porphyritic enclaves show the highest range in MnO contents, ranging from 0,14-0,26 wt%. K_2O and Na_2O display a smooth increasing trend. Also in the Na_2O diagram, the most variations can be noticed in the post horseshoe structure porphyritic enclaves. The P_2O_5 diagram normally shows an inclination when apatite starts to crystallize. The SiO2 versus Al_2O_3 diagrams shows the same trend when plagioclase starts to crystallize, this 'normal' trend cannot be observed in this dataset.

The large ion lithophile elements (LILE) all show different trends; Barium has an increasing trend with increasing SiO_2 because it does not favor any mineral. Strontium is favored by plagioclase and is scattered between 200-400 ppm. Lead also displays a positive correlation with SiO2, although with more scatter than barium.

The High field strength elements (HFSE) niobium and zirconium both show an increasing trend with increasing SiO_2. Yttrium is mainly decreasing but has some aberrant points which mainly consist of post horseshoe structure porphyritic enclaves. Cerium has mainly an increasing trend but has a lot more scatter, this scatter could also show an increasing trend because cerium has a large measurement error.

4.3 Bivariate ratio plots

Bivariate ratio plots were made of :

1. SiO_2 against Th/Nb, Zr/Nband K/Sr.
2. Y/Nb against Th/Nb and Zr/Nb.
3. Th against Ba/Th, Sr/Th, Cr/Th, V/Th and Ni/Th.
4. Sc/Cr againstV/Ni, Th/Nb against Rb/La, Sc/Th against K/Rb and Cr/Nb against Sr/Ba.

The results are shown in figure 13, 14 and 15.

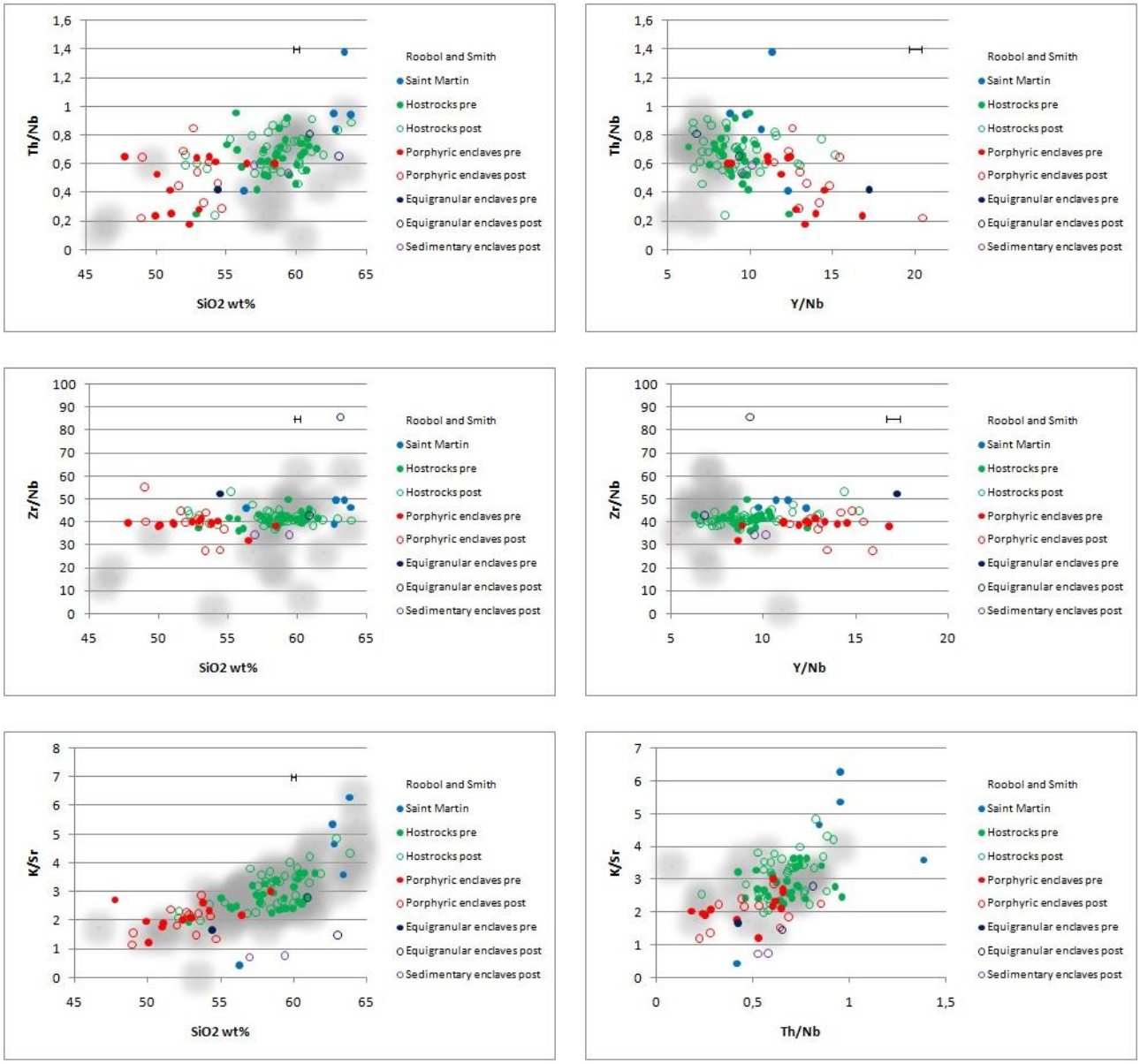

Figure 13: Zr/Nb displlays a constant ratio with increasing SiO_2 contents and Y/Nb ratios. Y/Nb ratios are higher for enclaves than for hostrocks. Th/Nb shows a lot of scatter. K/Sr is increasing with increasing SiO_2 content.

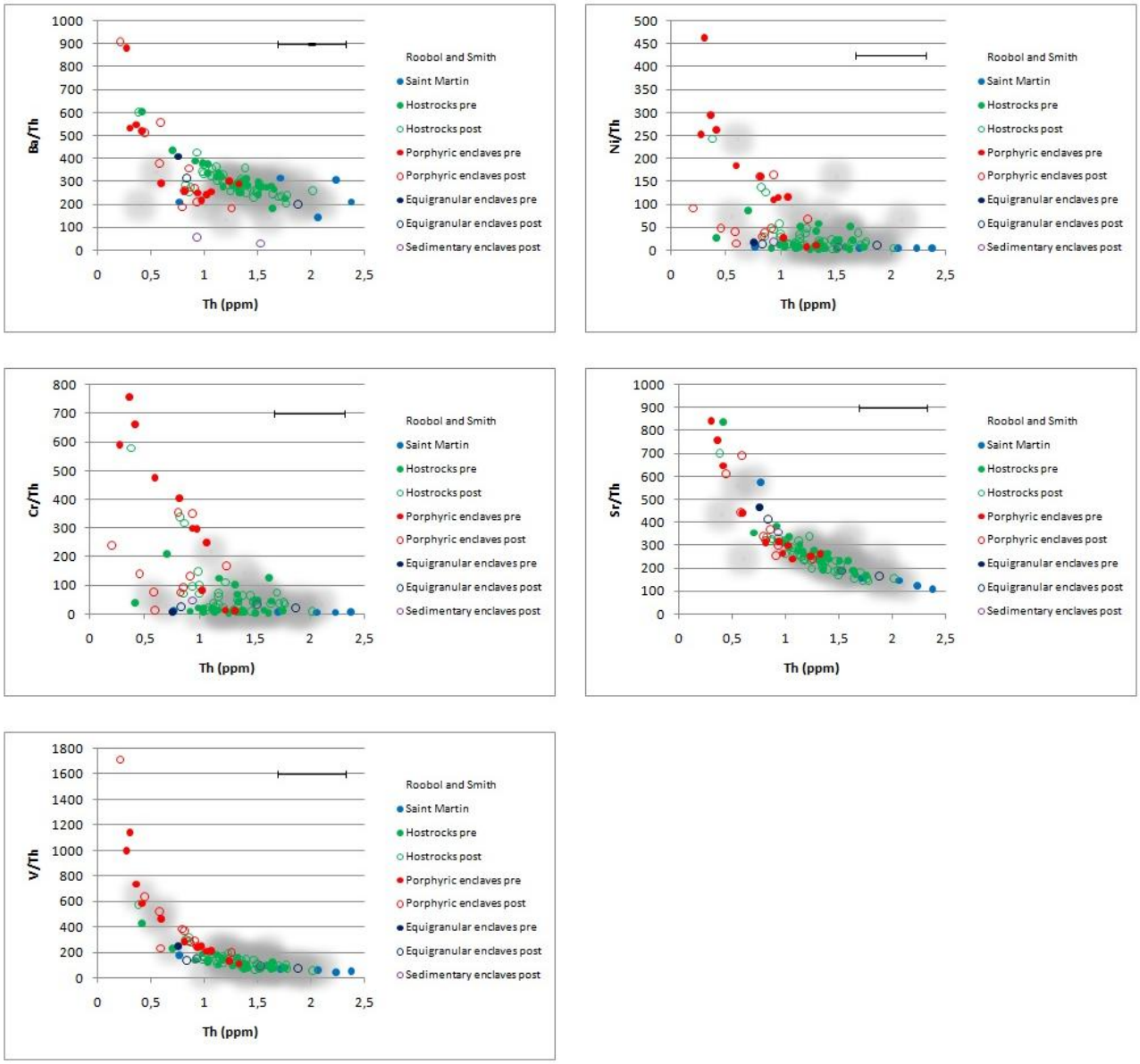

Figure 14: Cr/Th and Ni/Th show similar trends. Sr/Th and V/Th also show similar trends. Hostrocks show higher Th contents then enclaves.

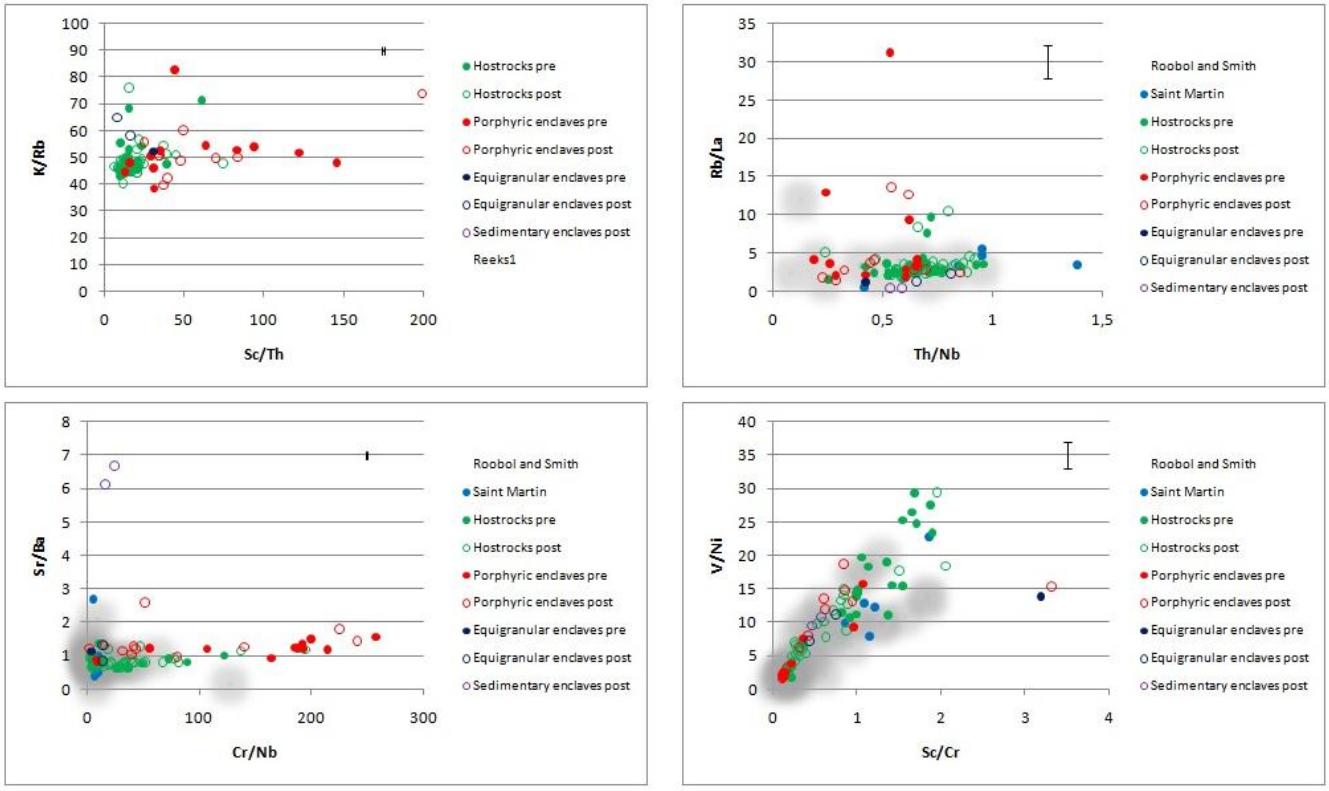

Figure 15: These diagrams show very different trends, they will be discussed in more detail in Chapter 5. Cr/Nb vs Sr/Ba is probably heavily influenced by fractional crystallization of clinopyroxene.

4.4 Isotope ratios of whole rocks and plagioclase

$^{87}Sr/^{86}Sr$ measurements were done for eight whole rock samples and ten picked plagioclase samples. In figure 16 the $^{87}Sr/^{86}Sr$ values are shown. In figure 17 SiO_2 versus $^{87}Sr/^{86}Sr$ of the plagioclase and whole rock is shown. No distinction can be made between pre- and post horseshoe structure volcanics. Therefore, the data points are subdivided into whole rock host, whole rock enclave, plagioclase host and plagioclase enclave.

Note that whole rock analysis gives higher $^{87}Sr/^{86}Sr$ values for hostrocks than for enclaves. For the plagioclase $^{87}Sr/^{86}Sr$ analysis this distinction cannot be made; hostrocks as well as enclaves vary between 0,7037 and 0,7038. $^{87}Sr/^{86}Sr$ values of two rocks were measured for both whole rocks and plagioclase (figure 16), in this case the whole rock values are higher than the plagioclase values. The limited number of whole rock analyses shows that the $^{87}Sr/^{86}Sr$ values decrease with increasing SiO_2 content. The enclave with high SiO_2 content is equigranular, the enclaves are porphyritic. It is clear that $^{87}Sr/^{86}Sr$ values for plagioclase show less variation than $^{87}Sr/^{86}Sr$ values of whole rocks.

In figure 18 $^{87}Sr/^{86}Sr$ values are plotted against LOI. With a normal alteration trend the $^{87}Sr/^{86}Sr$ values should increase with increasing LOI value. The $^{87}Sr/^{86}Sr$ values of these rocks are not influenced by alteration because the highest LOI value gives the lowest$^{87}Sr/^{86}Sr$ value.

$^{143}Nd/^{144}Nd$ were also done for the eight whole rock samples. In Figure 18 the results are plotted against $^{87}Sr/^{86}Sr$. Note that $^{143}Nd/^{144}Nd$ ratios lie very close to Atlantic MORB values (0,51303-0,51282[4]).

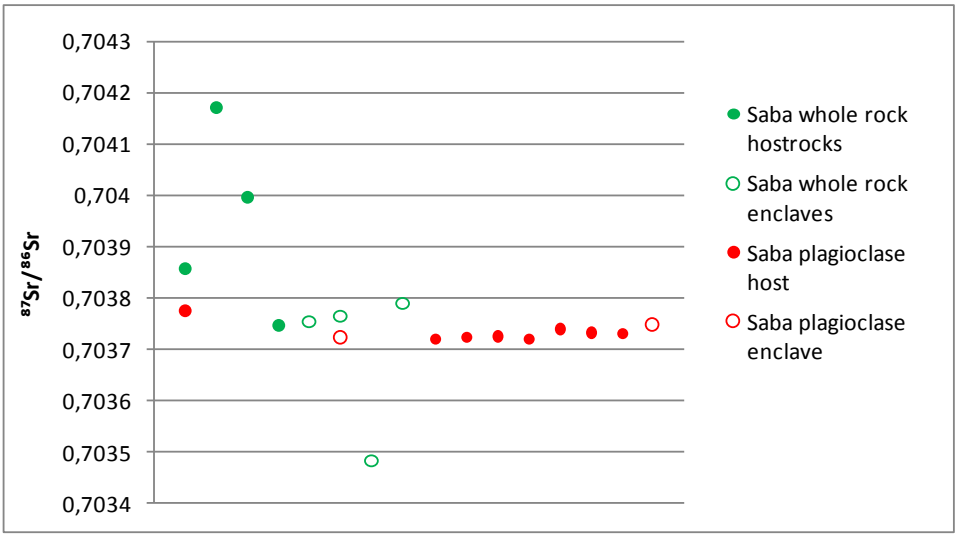

Figure 16: $^{87}Sr/^{86}Sr$ values of whole rocks (green) and plagioclases (red).

[4]data obtained from Le Roux, 1987

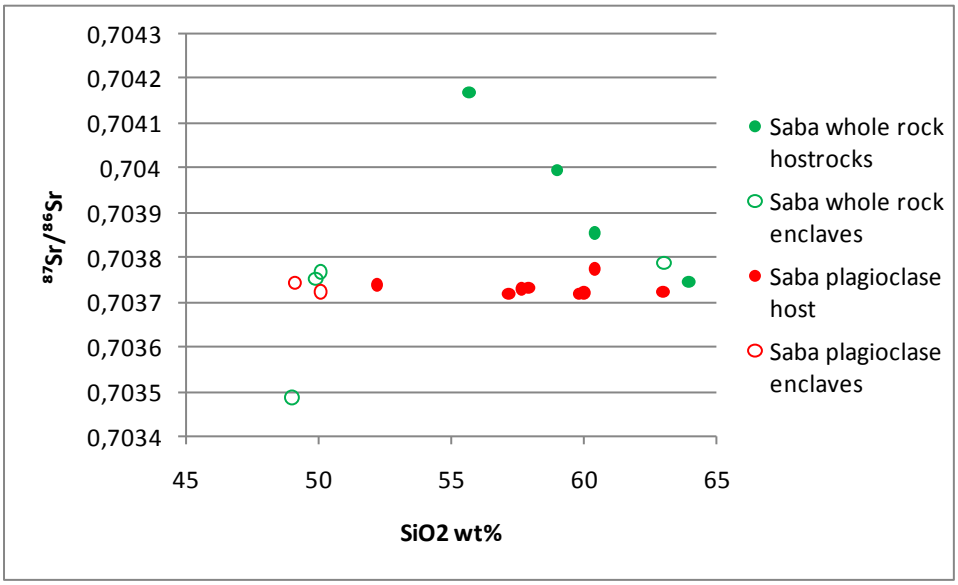

Figure 19: $^{87}Sr/^{86}Sr$ values of whole rocks (green) and plagioclases (red) against SiO_2 contents of whole rock compositions

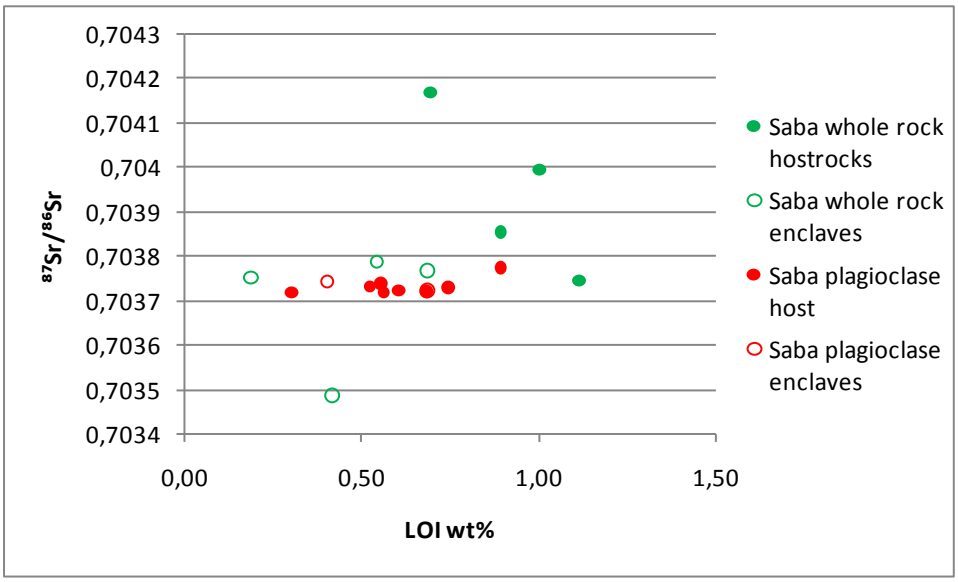

Figure 18: $^{87}Sr/^{86}Sr$ values of Saba hostrocks (green) and Saba enclaves (red) against LOI

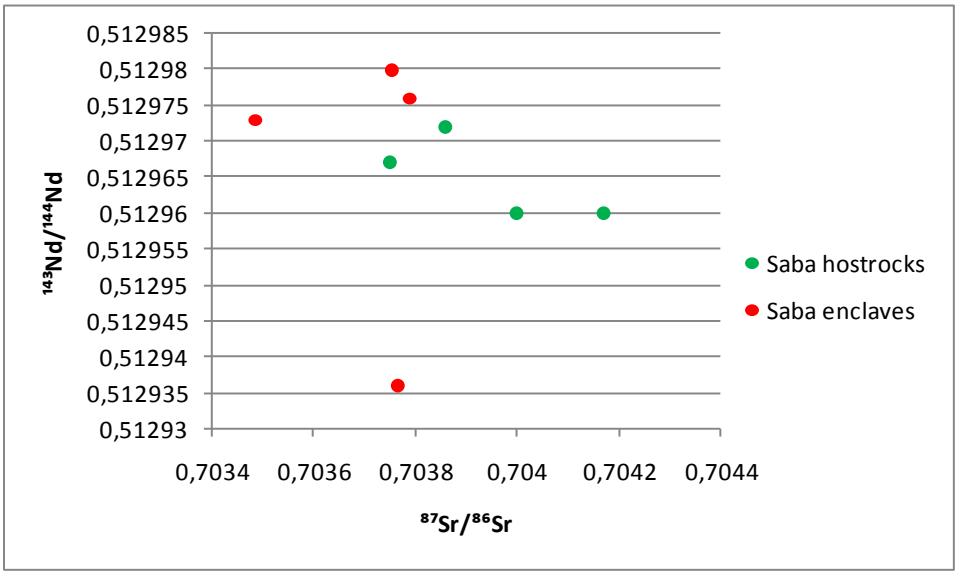

Figure 17: $^{87}Sr/^{86}Sr$ values of whole rocks (green) and plagioclases (red) against $^{143}Nd/^{144}Nd$

Chapter 5: Discussion

5.1 Mixing melts

On both the macroscopic, microscopic and geochemical scale it is clear that magma mixing occurs underneath Saba. As shown in Figure 10, nearly all the volcanic rocks contain evidence like mingling and mafic enclaves on macroscopic scale. Figure 20 shows that boundaries between hostrocks and enclaves are also visible on microscopic scale. As shown in Figure 11 and Figure 12, there is a clear distinction in SiO_2 content between hostrocks and enclaves. For this reason, the aim of this discussion is to find out the composition and possible source of the end member magmas.

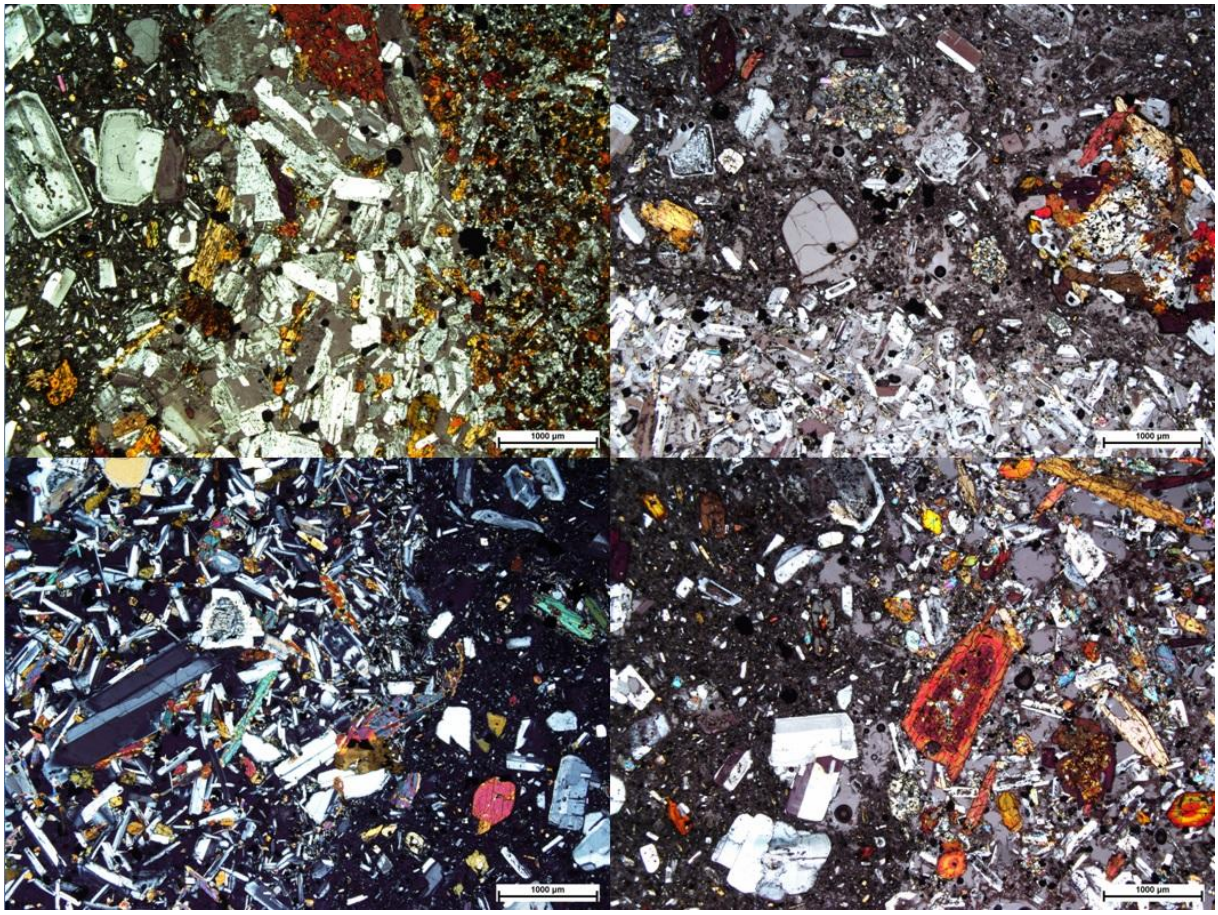

Figure 20: Microscopic mixing evidence: boundaries between hosts and enclaves of SB003, SB024AI, SB033BI and SB056II.

For testing whether mixing is a viable process the mixing equation of Langmuir et al. (1978) can be used. The mixing equation is hyperbolic and has the form:

$$Ax + Bxy + Cy + D = 0 \qquad [1]$$

The equation is used for ratio-ratio plots where the coefficients for the equation become:

$A = a_2b_1y_2 - a_1b_2y_1$

$B = a_1b_2 - a_2b_1$

$C = a_2b_1x_1 - a_1b_2x_2$
$D = a_1b_2x_2y_1 - a_2b_1x_1y_2$

For ratio-element plots the coefficients for the equation become:
$A= a_2y_2 - a_1y_1$
$B= a_1 - a_2$
$C=a_2x_1 - a_1x_2$
$D= a_1x_2y_1 - a_2x_1y_2$

Symbols used are x,y = general variables along the abscissa and ordinate, a*i* = denominater of y*i*, b*i* = denominator of x*i*. The equation predicts that mixing between two ratios produces an asymptotic curve. There are two different types of mixing. The first type is mixing of sources, this means mixing occurred in the source before melting. The second type is mixing/mingling of magmas, this means mixing between magmas occurred after their separation as melt from their sources. These two types can be differentiated by using differences in the behavior between compatible and incompatible elements. Compatible element ratios are strongly fractionated during partial melting and will not reflect the ratios of the source region. Partial melting and differentiation do not affect the ratios of incompatible elements. If mixing occurs in the source region a compatible element plot will show a scattered trend while it shows a simple line when mixing of two magmas occurs. Incompatible element plots should show relations for both mixing of magmas and mixing of sources (Langmuir et al. 1978).

Equation [1] is used in bivariate ratio diagrams of Y/Nb against Th/Nb and Zr/Nb, K/Rb against Th/Nb, Sc/Cr againstV/Ni, Th/Nb against Rb/La, Sc/Th against K/Rb and Cr/Nb against Sr/Ba.

As mixing end members the felsic hostrock SB024AII and the two mafic enclaves SB021B and SB024BII are used. These rocks are assumed to represent the three different end members the best. SB024AII has a SiO_2 content of 63,9 wt % and a Th content of 2,0 ppm. SB024BII is a post horseshoe structure volcanic and has a SiO_2 content of 49,0wt % and a Th content of 0,2 ppm. SB021B is a pre horseshoe structure volcanic and has a SiO_2 content of 49,9 wt% and a Th content of 0,3 ppm. The results are shown in figure 21-27. The felsic component could be the result of long term fractional crystallization in the magma chamber and represents the upper part of the magma chamber where felsic minerals float on top of a more mafic melt.

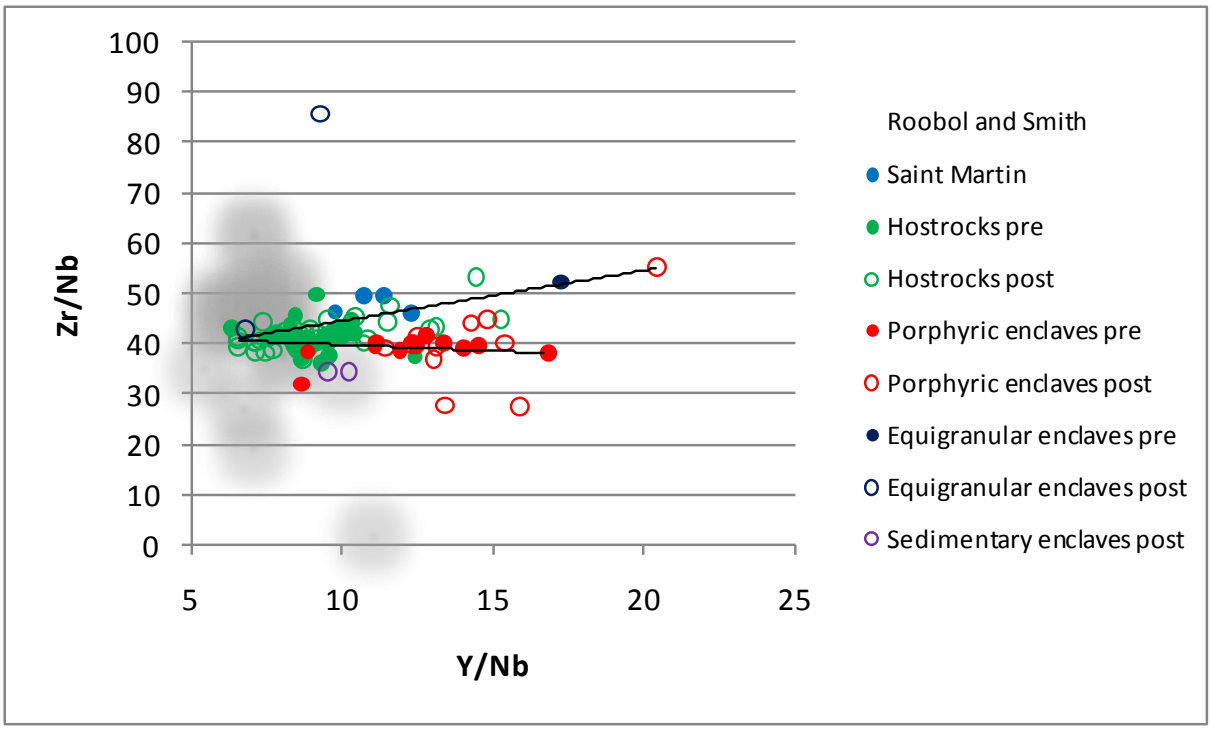

Figure 21: The mixing line from the post horseshoe structure mafic enclave (SB024BII) does not fit with the data points. The mixing line from the pre horseshoe structure mafic enclave (SB021B) fits with most of the pre horseshoe structure data points.

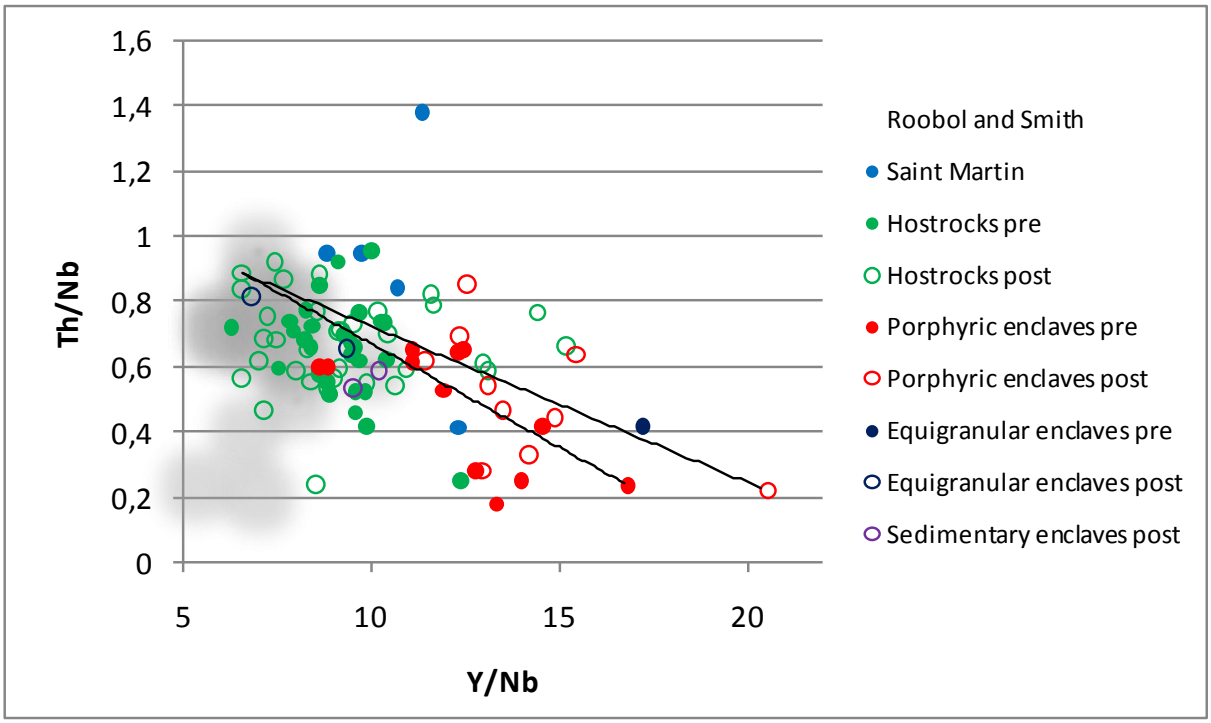

Figure 22: The data in this diagram are very scattered. The mixing lines are located in the center of the scatter so could explain mixing but obviously some other processes could work as well.

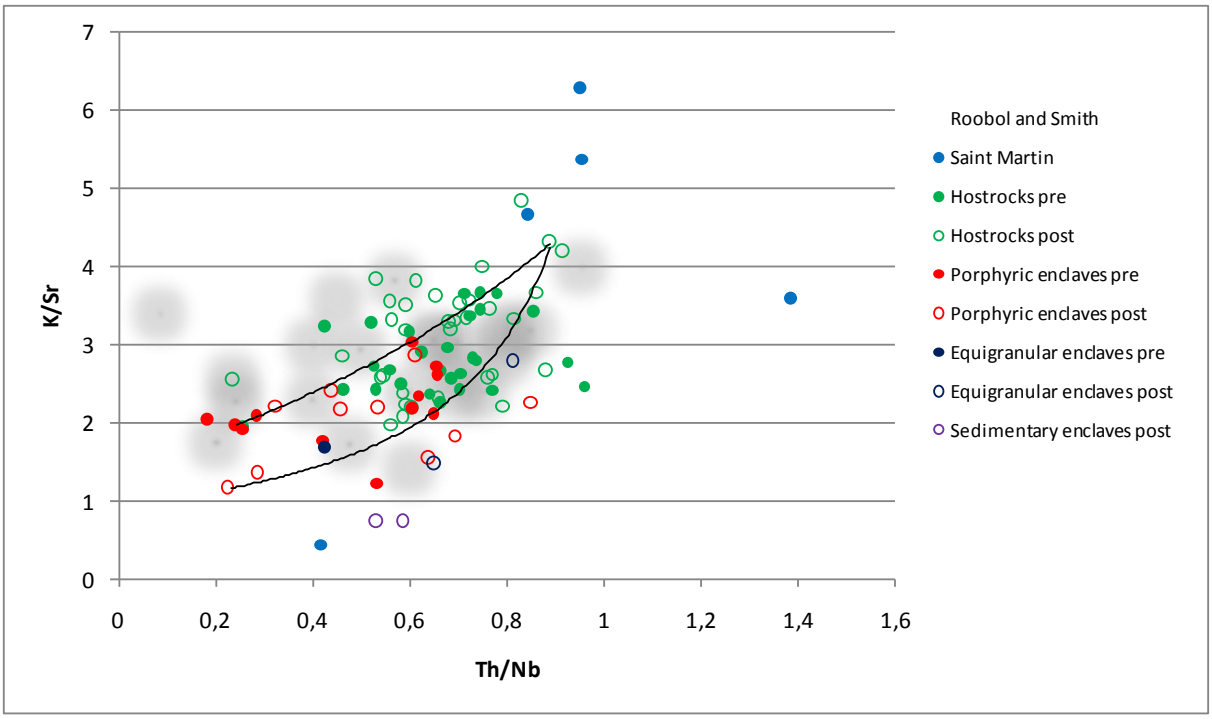

Figure 23: The data in this diagram are very scattered. The mixing lines are located in the center of the scatter so could explain mixing but obviously some other processes could also explain the data. All the elements in this plot are incompatible so the scatter could be caused by both mixing of magmas as mixing of sources.

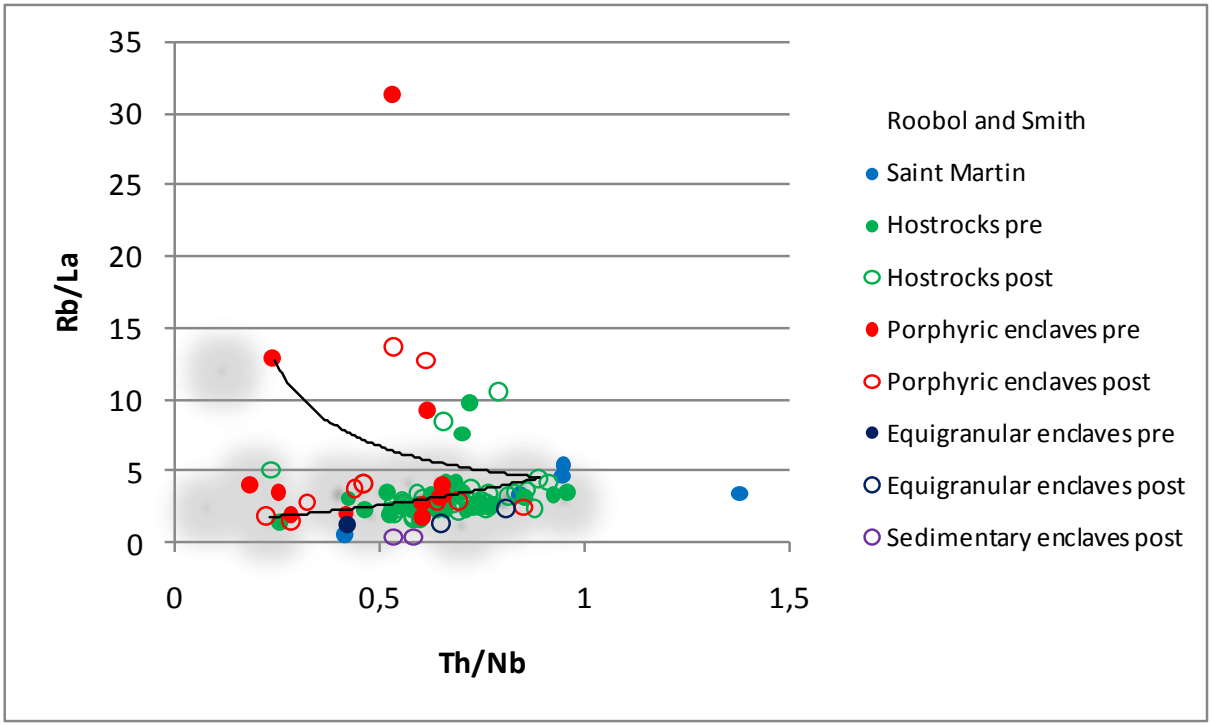

Figure 24: Most of the data seem to follow the mixing curve of the post horseshoe structure mafic enclave (SB024BII). The rocks with high Rb/La ratios have very low La concentrations, the other element concentrations in these rocks are comparable to other Saba volcanics.

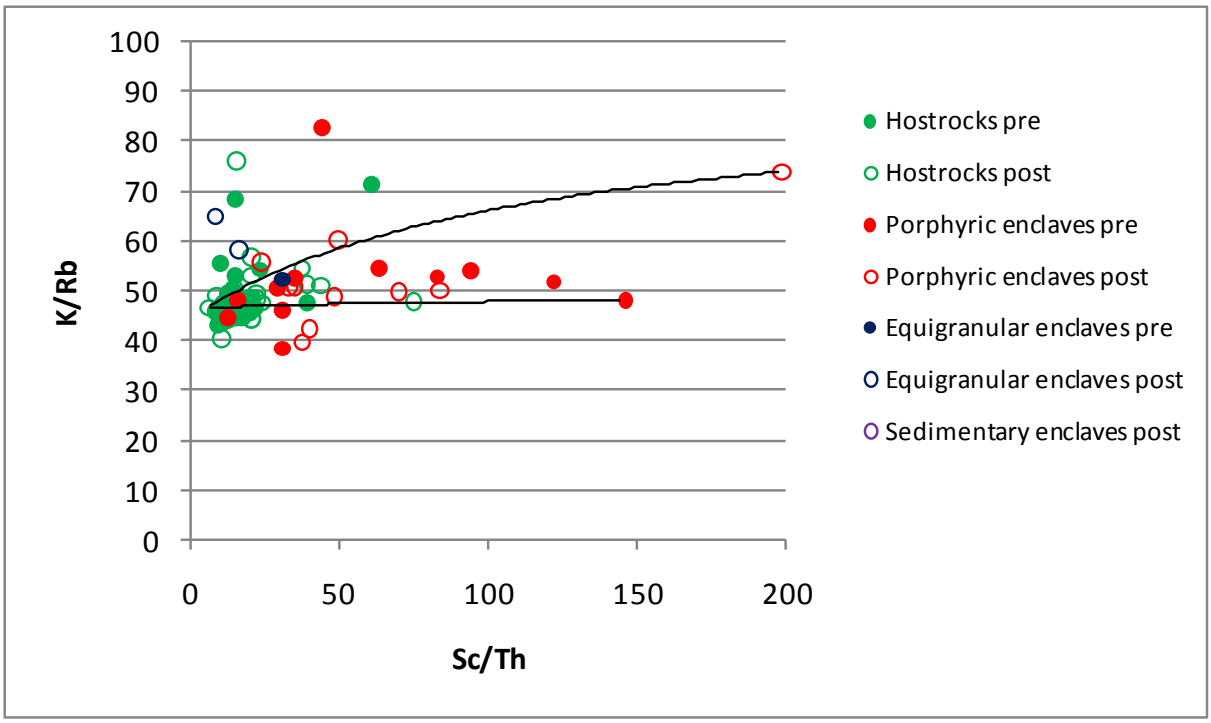

Figure 25: The mixing line of SB024BII does not fit with the data points. Although the data falls slightly off the mixing curve of SB021B, this mixing line seems to represent the mixing between pre horseshoe structure enclaves and the felsic SB024AII.

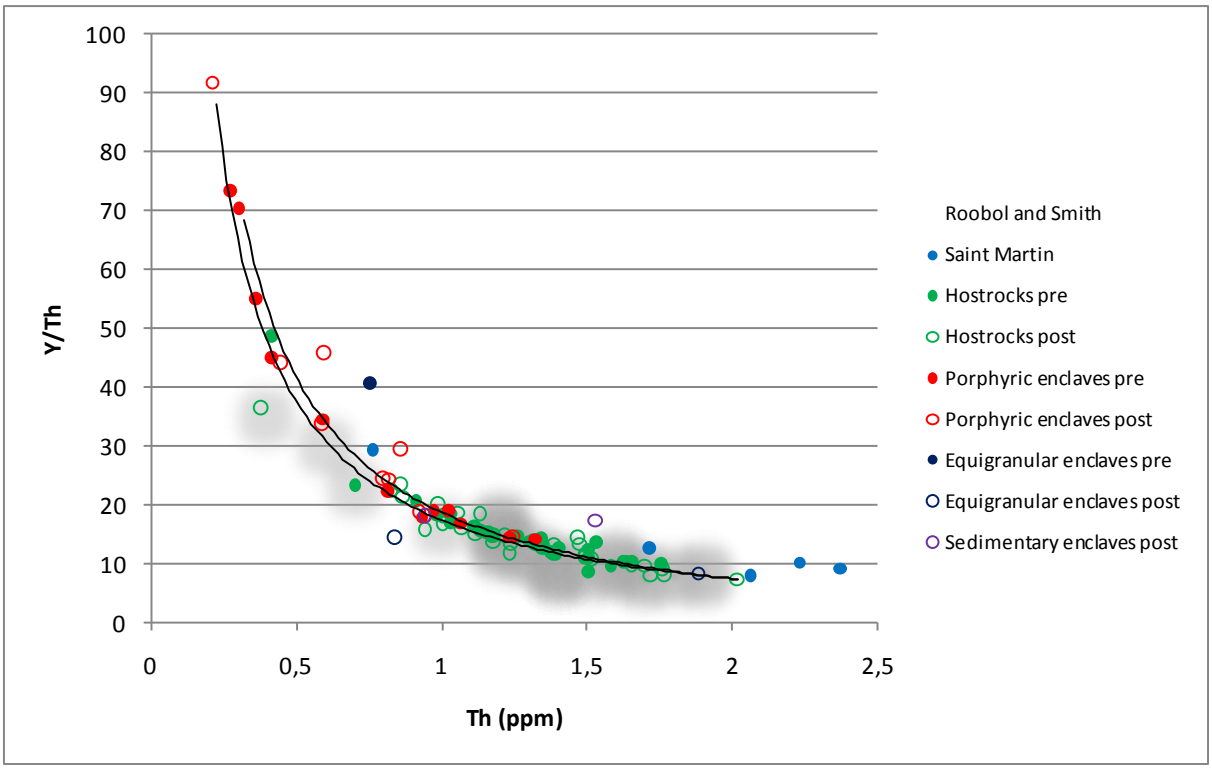

Figure 26: If mixing between SB024AII and SB024BII/SB021B (or their sources) is responsible for the trend in Saba volcanics, the exact ratios for each end member can be determined using this diagram. Most hostrocks lie between a mixture of 88% felsic component with 12% mafic component and 38%felsic component with 62%mafic component. Enclaves contain more mafic component although the group of enclaves located in the middle of the diagram is 50-50% influenced by both end members.

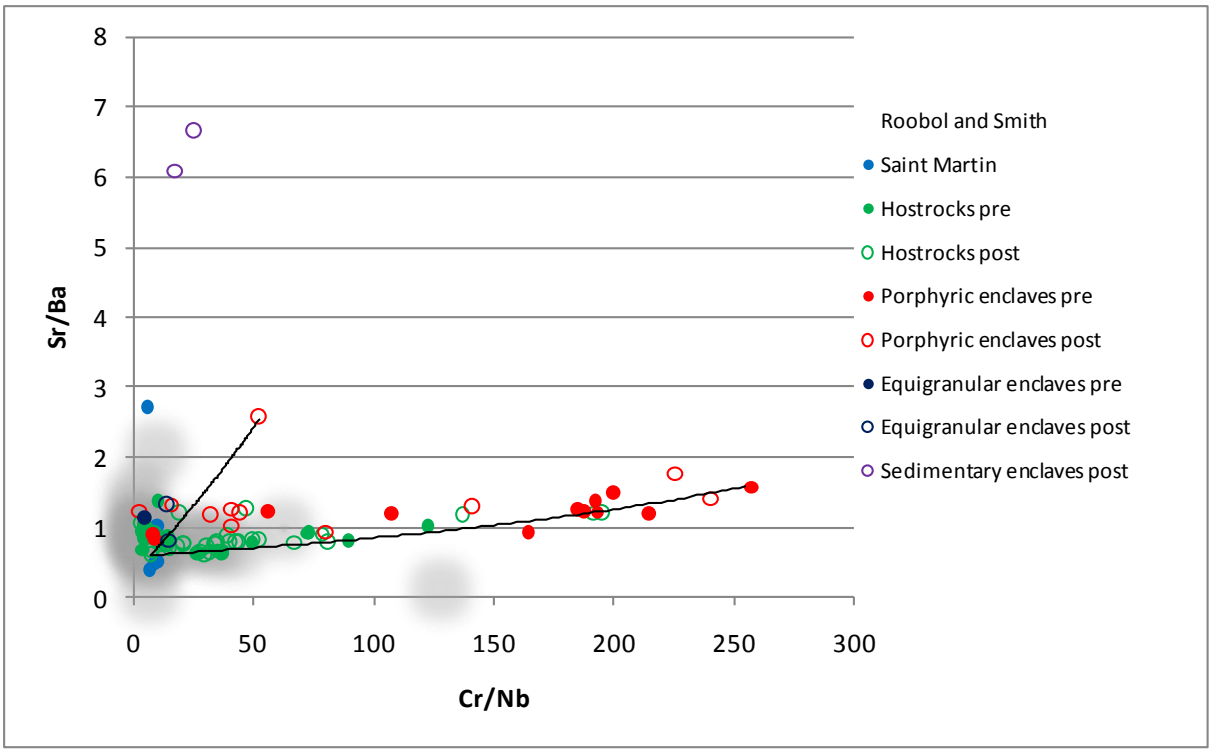

Figure 27: The mixing line of SB024BII does not fit with the data points whereas the mixing line of SB021B has a very good fit with the data points.

Most of the data have a better fit with the mixing curve of the pre horseshoe structure rock SB021B instead of the post horseshoe structure rock SB024BII. Therefore it can be concluded that SB021B and SB024AII are the best representations of the two mixing end members. Table 5 gives the chemical composition of SB021B and SB024AII. Thin section photos of SB024AII and SB021B are shown in figure 28 and figure 29.

	SB021B	SB024A II		SB021B	SB024A II
FeO	7,87	4,44	Er	2,17	2,61
MnO	0,15	0,14	Ni	139,49	11,29
TiO_2	1,01	0,45	Yb	5,61	5,24
CaO	10,93	5,93	V	343,51	98,12
K2O	0,60	1,59	Cr	324,33	15,72
P2O5	0,09	0,12	Co	35,47	10,64
SiO2	49,92	63,94	Ba	160,19	521,25
Al_2O_3	17,77	16,86	Sc	43,71	13,79
MgO	9,05	2,17	Hf	1,92	1,05
Na_2O	2,58	3,70	Mo	1,05	2,05
BaO	0,02	0,06	Nb	1,26	2,27
			Y	21,17	14,99
La	0,80	6,22	Zr	48,26	92,71
Ce	6,74	19,41	Sr	252,99	307,63
Nd	8,19	11,12	Rb	10,33	28,29
Sm	2,32	2,12	Th	0,30	2,02
Ga	16,38	15,98	Pb	0,33	3,30
Zn	62,02	51,10			
Cu	145,25	30,51	$^{143}Nd/^{144}Nd$	0,51298	0,512967
Hf	1,56	2,93	$^{87}Sr/^{86}Sr$	0,703754	0,703747

Table 5: Chemical composition of the mafic mixing component SB021B and the felsic mixing component SB024AII.

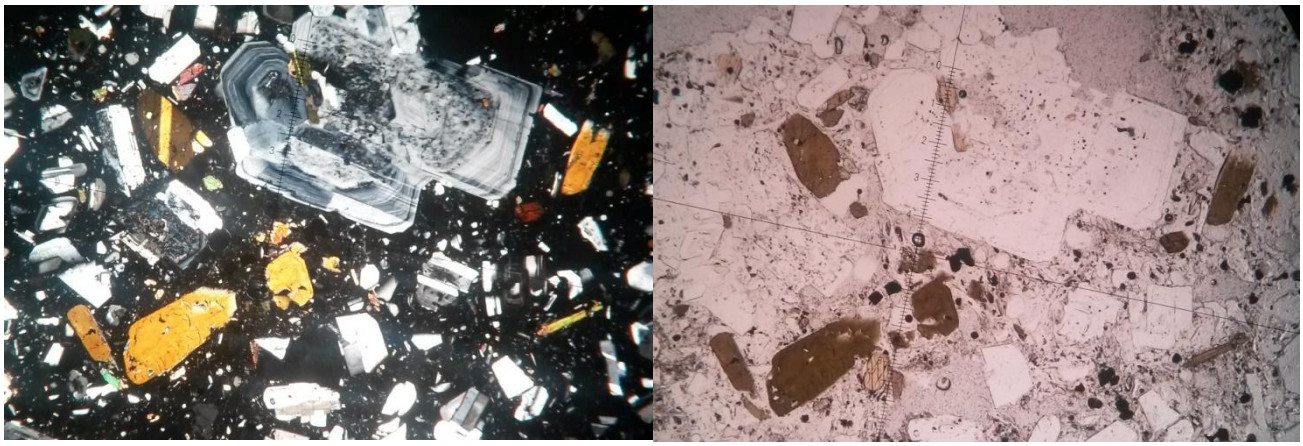

Figure 29: Thin section photos of SB024AII. This hostrock has a very fine grained matrix. The phenocrysts consists of plagioclase (65%), amphibole (30%) and opaque minerals (5%). Around 5-10% of the plagioclase phenocrysts contain sieve textures but most of them are unaltered.

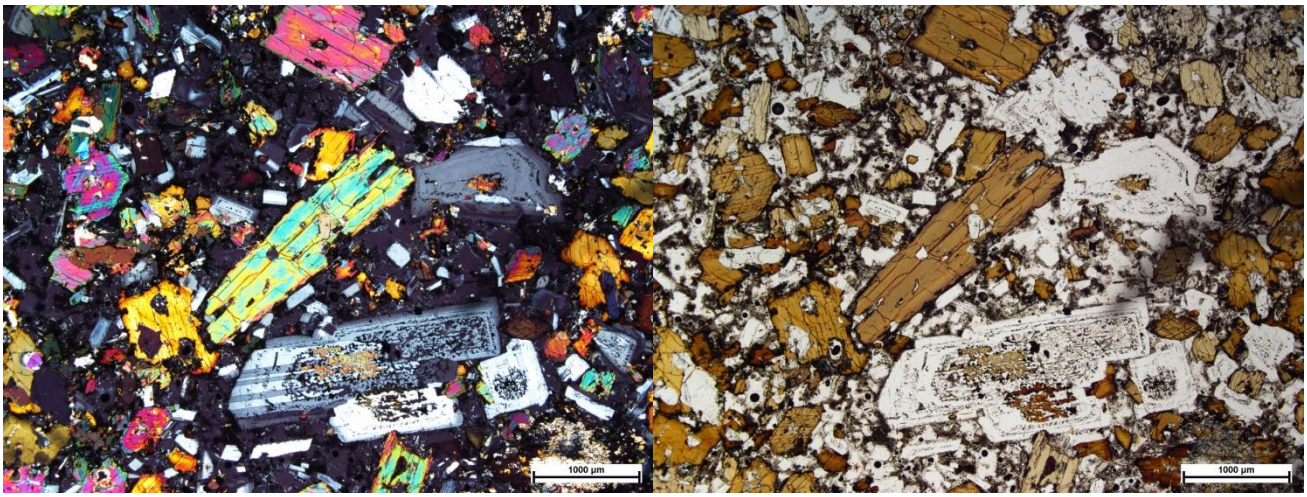

Figure 28: Thin section photos of SB021B. Porphyritic basaltic enclave with phenocrysts of amphibole (60%) and plagioclase (40%). Some of the phenocrysts are fragmented. The groundmass consists mainly of plagioclase (70%). Other minor minerals are olivine, clinopyroxene and opaque minerals. Note that most plagioclase phenocrysts have sieve textures.

Although the mixing curves in the figures 21-27 cannot fully explain the location of the data points, it is clear that mixing occurs in the magma chamber(s) of Saba. Still a lot of data points cannot be explained, this indicates that different magmatic processes are affecting the geochemical signature of the rocks at the same time. Therefore fractional crystallization and assimilation processes will be discussed in paragraph 5.2 and 5.3.

5.2 Fractional crystallization

Magmatic rocks experience differentiation processes in a magma chamber prior to their emplacement at the surface. These processes modify the chemical composition of the primary magma (mafic component) which is produced by partial melting of the source. Processes that differentiate the mafic magma to a felsic magma could be fractional crystallization, magma mixing and assimilation. In most cases, a combination of these processes occur. In this paragraph the focus lies on fractional crystallization because this is the most common and easy process to recognize.

Bivariate vector diagrams of Th versus Ba/Th, Sr/Th, Cr/Th, V/Th and Ni/Th are shown in figure 30-34. In these diagrams vectors of plagioclase (purple), amphibole (black) and clinopyroxene (blue) are added. A olivine vector (green) is also added to the Th versus Ni/Th and Th versus Cr/Th diagram. Vectors were constructed using the formula:

$$\frac{C_L}{C_O} = F^{(D-1)} \qquad [2]$$

Where C_L is the residual liquid, C_O is the concentration of the element in the original magma, F is the fraction of melt remaining after removal of crystals and D is the distribution coefficient. Distribution coefficients are obtained from Rollinson (1993) and earthref.org (table 6). F is shown above each diagram. Sample SB039I is used for the initial melt values (C_O) because this is the most mafic hostrock with a SiO_2 content of 52,2 wt% and a MgO content of 7,6 wt%.

	Th	Sr	Ba	Cr	Ni	V
plagioclase	0,01	1,83	0,23	0,02	0,1	0,025
clinopyroxene	0,03	0,06	0,026	34	6	1,35
amphibole	0,5	0,46	0,42	12,5	6,8	3,4
olivine	0,01	0,014	0,0099	0,7	10	0,06

Table 6: Distribution coefficients for plagioclase, clinopyroxene, amphibole and olivine used in fractional crystallization and AFC models. All distribution coefficients are from Rollinson (1993).

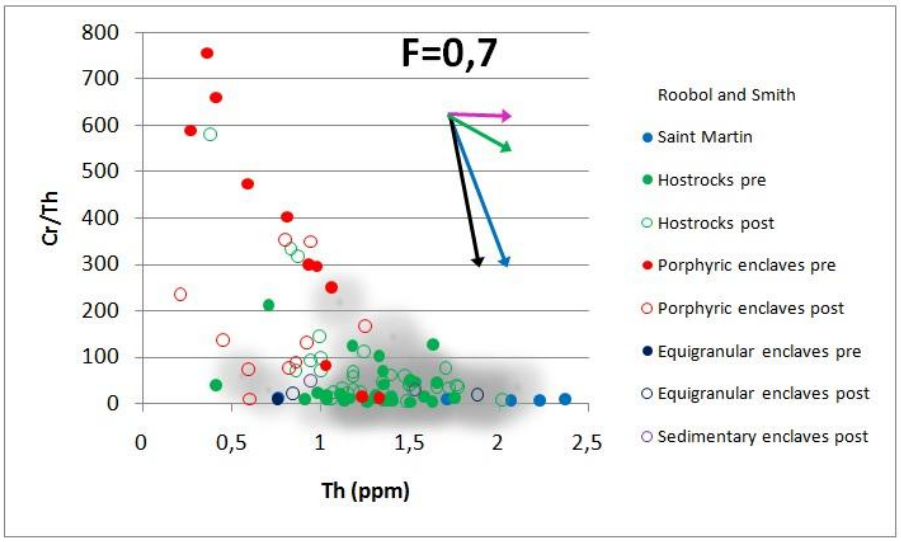

Figure 30: Vector diagram of Th versus Cr/Th
Vectors: Purple=plagioclase, black=amphibole, blue=clinopyroxene, green =olivine

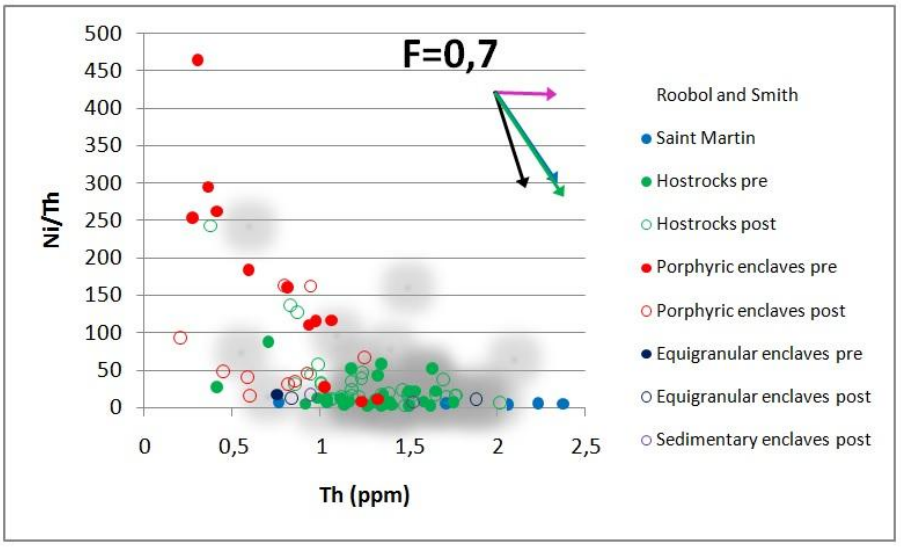

Figure 31: Vector diagram of Th versus Ni/Th
Vectors: Purple=plagioclase, black=amphibole, blue=clinopyroxene, green =olivine

Cr and Ni are favored by clinopyroxene and olivine. Hornblende can also influence the Cr and Ni abundances. Most hostrocks have low Cr/Th and Ni/Th values so they are likely influenced by fractional crystallization of these minerals.

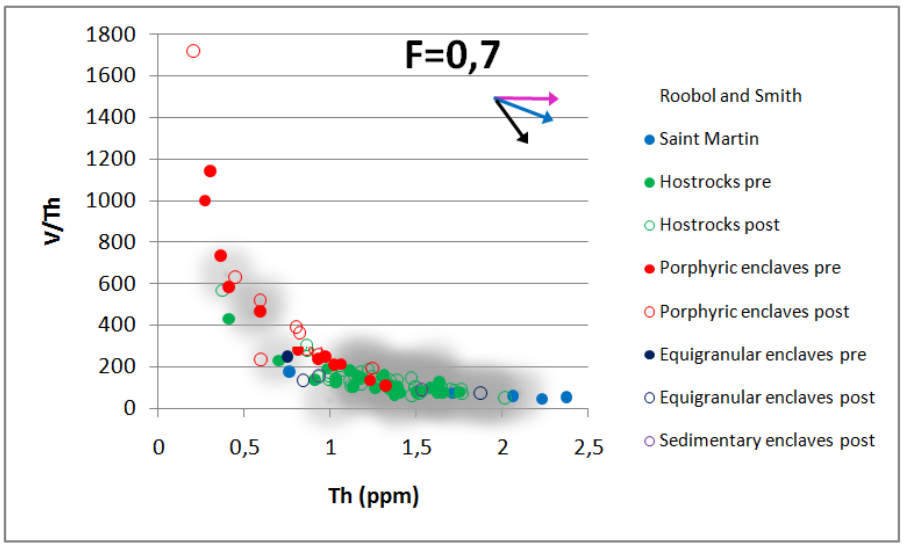

Figure 32: Vector diagram of Th versus V/Th
Vectors: Purple=plagioclase, black=amphibole, blue=clinopyroxene

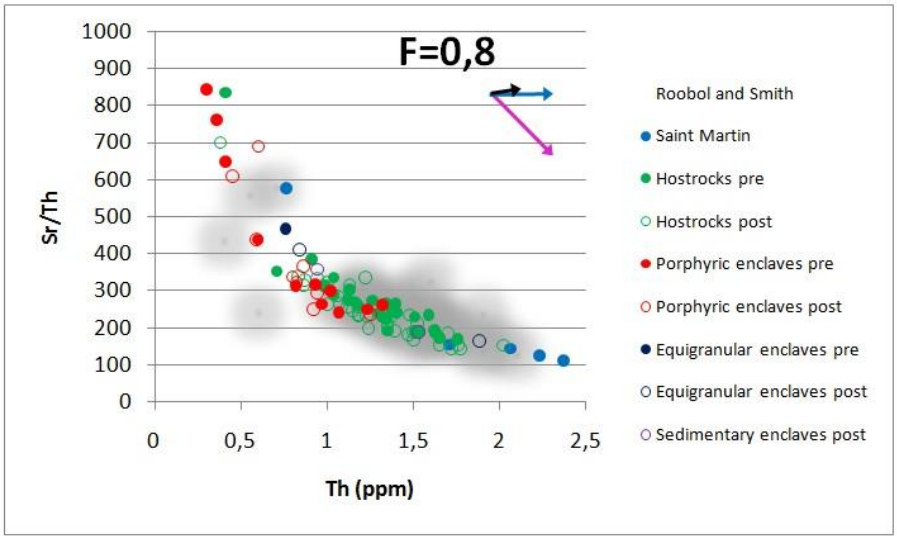

Figure 33: Vector diagram of Th versus Sr/Th
Vectors: Purple=plagioclase, black=amphibole, blue=clinopyroxene

In the V/Th diagram plagioclase seems to have no influence and the trend can mainly be explained by the crystallization of clinopyroxene. V is favored by hornblende and clinopyroxene. Note that amphibole shows a steeper trend than clinopyroxene and the trend is steeper for the enclaves than for the hostrocks. Most amphibole is found in enclaves. Sr is favored by plagioclase but unfortunately the trend cannot be explained by crystallization of plagioclase.

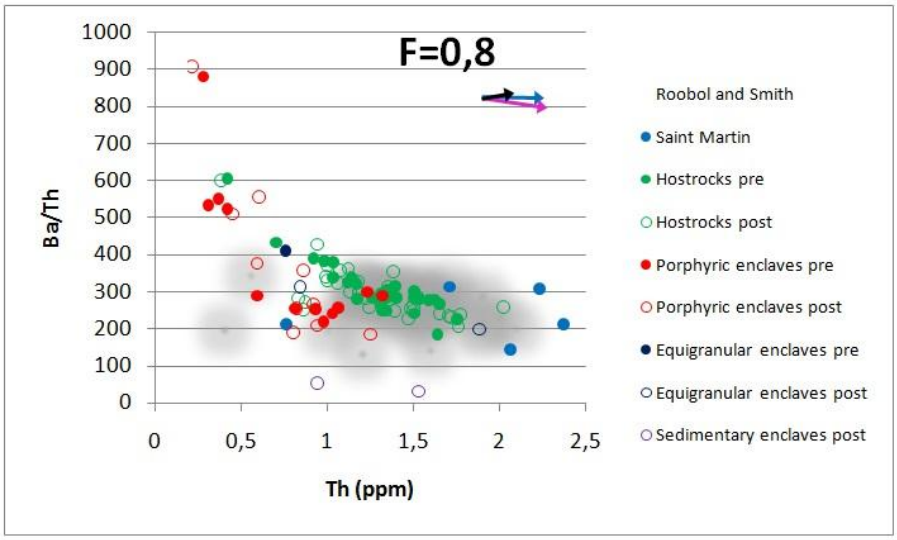

Figure 34: Vector diagram of Th versus Ba/Th
Vectors: Purple=plagioclase, black=amphibole, blue=clinopyroxene

Barium and thorium are incompatible in all of the minerals so during fractional crystallization the Ba/Th value should stay the same. Note that in this diagram the Ba/Th ratio is decreasing by a factor 4 which is caused by a faster increasement in Th than in Ba. This could not be caused by fractional crystallization.

Although the element ratios are definitely influenced by the crystallization of olivine, plagioclase, hornblende and clinopyroxene, the complete mafic to felsic differentiation trends cannot be explained. Especially the fractionation of plagioclase seems to have no influence on the observed trends. Although plagioclase is very abundant in the rocks Sr values cannot be explained by fractionation of plagioclase. The Ba/Th ratio is decreasing while the fractional crystallization factors are almost horizontal, this cannot be explained by fractional crystallization. Therefore it is likely that a combination of fractional crystallization, mixing and assimilation influenced the differentiation trend. To be able to explain the Ba/Th ratio, the assimilant should have a low Ba content or high Th content.

5.3 Assimilation and Fractional Crystallization (AFC)

According to Bowen (1928) assimilation of wallrock is driven by the latent heat of crystallization during fractional crystallization. Consequently, the processes are working at the same time named Assimilation and Fractional Crystallization processes (AFC). DePaolo (1981) derived equations which describe the concentration of a trace element in a melt relative to the original magma composition in terms of AFC processes. To model the AFC processes in the Saba magmas some of these equations are used in diagrams. The following formula is used for the element ratios (DePaulo, 1981):

$$\frac{C_m}{C_m^\circ} = F^{-Z} + \left(\frac{r}{r-1}\right)\frac{Ca}{zC_m^\circ}(1 - F^{-z}) \quad [3]$$

Where C_m is the concentration of the element in the magma, C_m° is the original concentration in the magma, r is the assimilation rate divided by the crystallization rate, F is the mass of the magma

divided by the initial mass of the magma, Z = (r + D – 1)/ (r – 1) and D is the partition coefficient for the element.

As noted in paragraph 5.2 the Saba assimilant should have a low Ba content or high Th content to explain the Ba/Th ratio. High Th contents can be found in the upper continental crust. Low Ba contents are found in gabbroic lower crustal layers.

Ersoy and Helvaci (2010) created a FC-AFC and mixing modeler in Excel. This program is used to plot AFC diagrams. These diagrams were made for Rb/La versus Th/Nb, K/Sr versus Th/Nb, Th/Nb versus Y/Nb, Zr/Nb versus Y/Nb, Sr/Th versus Ba/Thand Sr/Th versus Ba/Nb (Fig 36-41). In these diagrams SB021B is used for the initial magma of the AFC curve. As assimilant upper continental crust values are used from Taylor and McLennan (1995). In every diagram the r value is 0,2. Because the program had also the ability to plot FC and mixing curves, these are also added. The input values are shown in figure 35. The results are shown in figure 36-41. Table 7 gives the geochemical composition of two different end members.

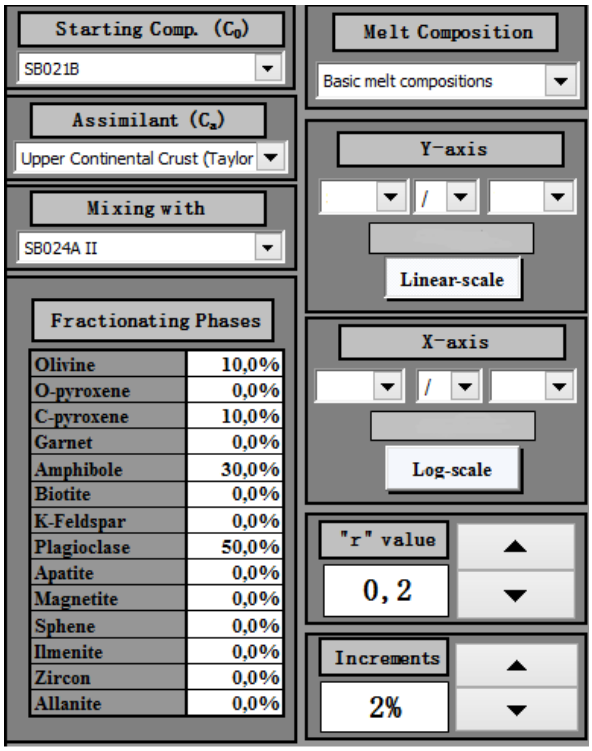

Figure 35: input values for the FC-AFC and mixing modeler

	North Atlantic Sediment	Upper Contental Crust
$^{87}Sr/^{86}Sr$	0,71788	0,704636
$^{143}Nd/^{144}Nd$	0,51193	0,513077
K_2O wt %	1,81	3,39
Rb ppm	83,5	112
Sr ppm	111	350
Ba ppm	204	550
Y ppm	23,9	22
Zr ppm	146	190
Nb ppm	18,33	25
La ppm	35,54	30
Nd ppm	31,22	26
Th ppm	12,08	10,7

Table 7: Possible assimilant data. Data obtained from Taylor and McLennan, 1985 and Plank and Langmuir, 1998.

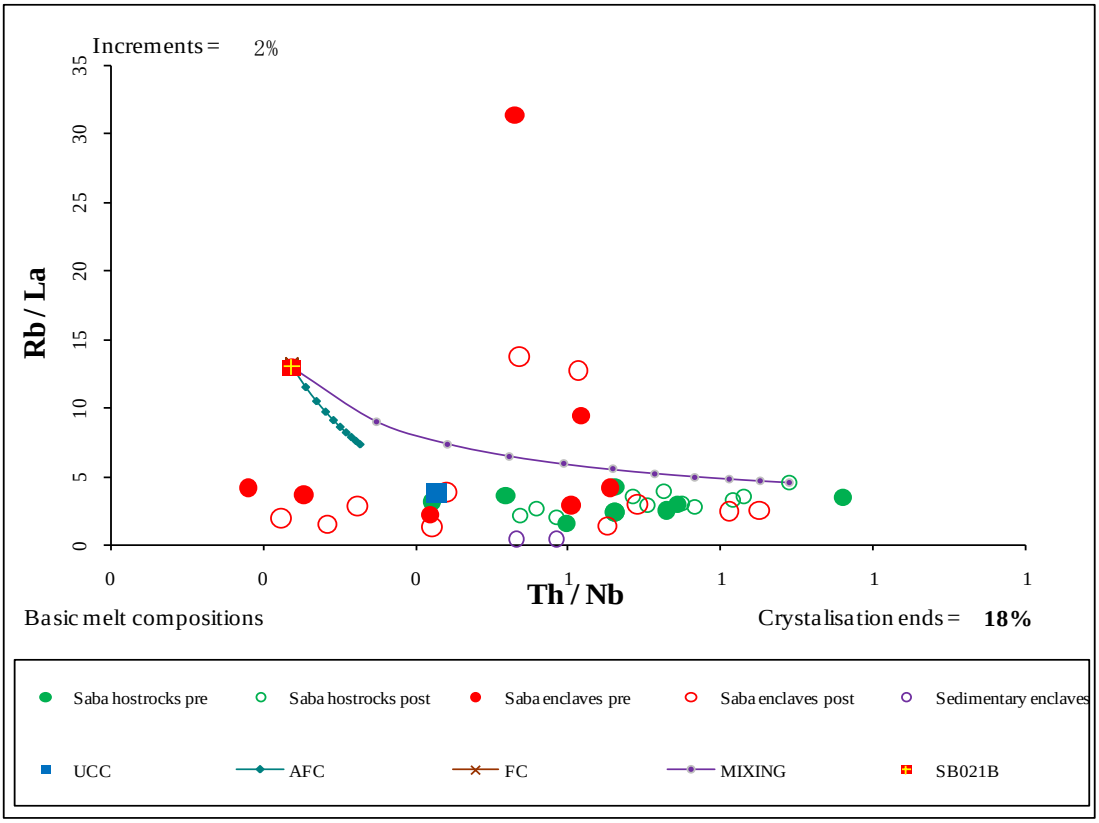

Figure 36: The data does not fit with the assimilation curve.

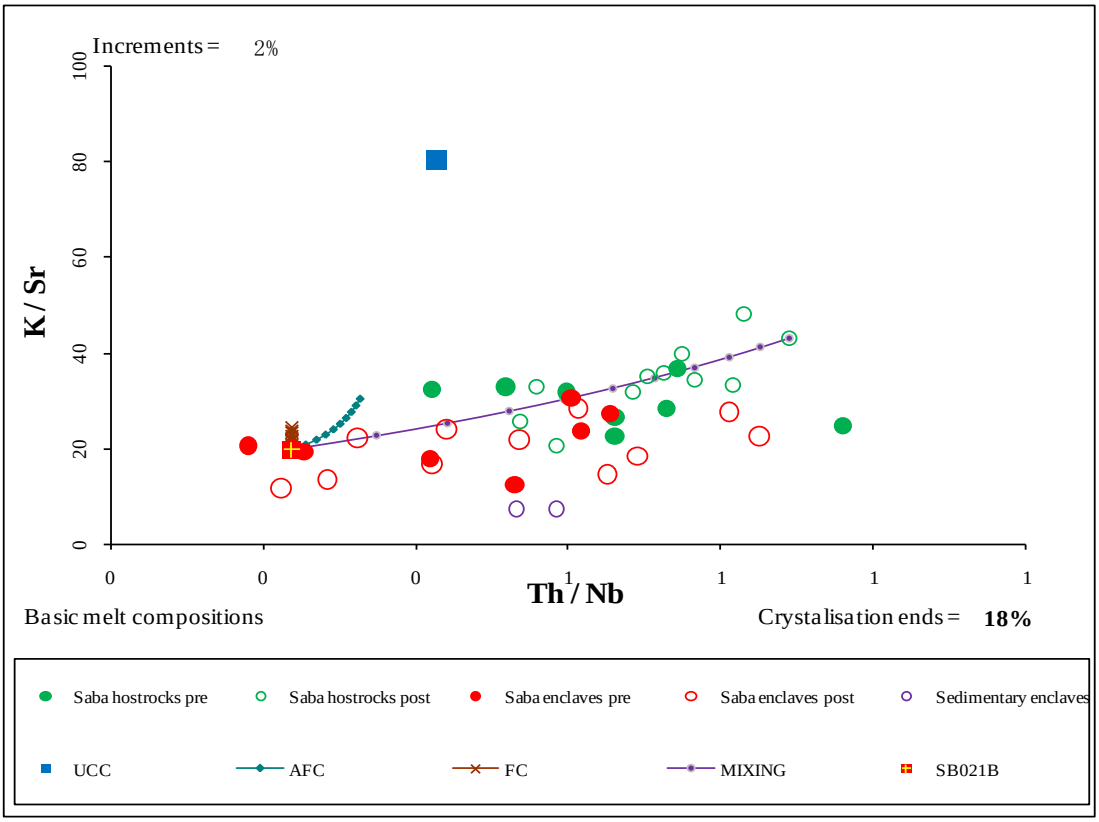

Figure 37: The data does not fit with the assimilation curve and has the best fit with the mixing curve.

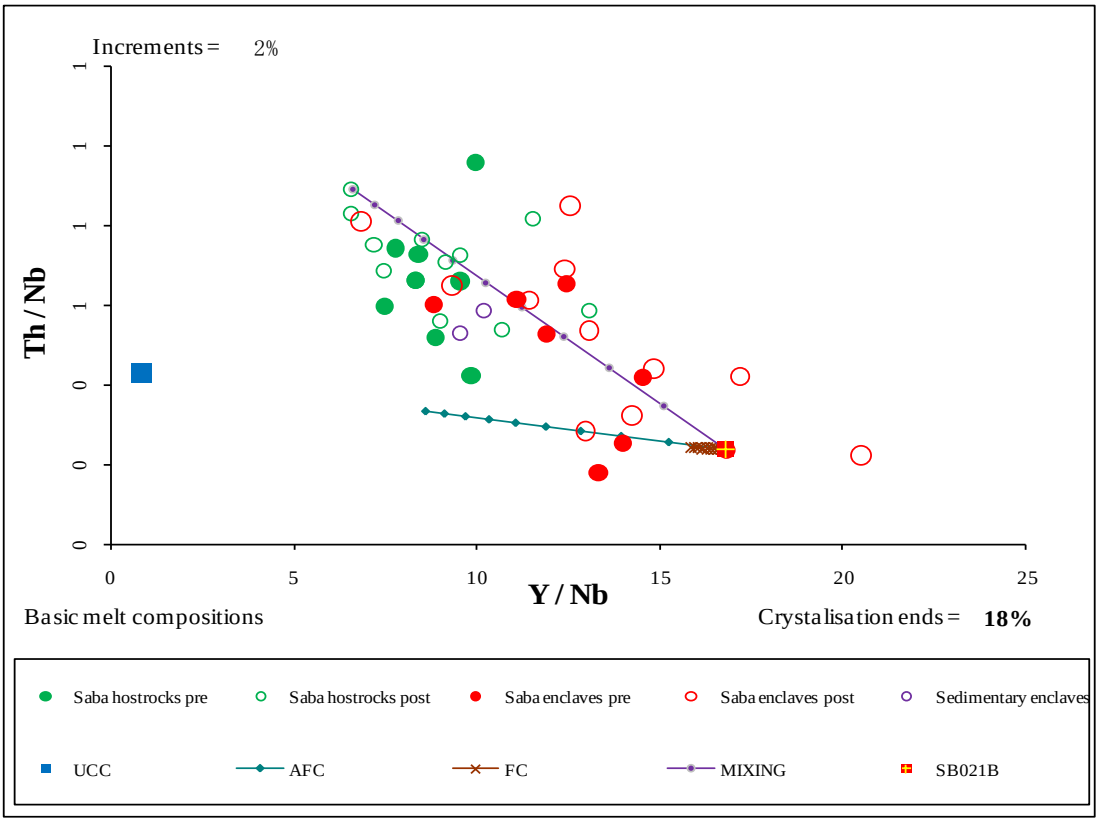

Figure 38: The data does not fit with the assimilation curve and has a better fit with the mixing curve.

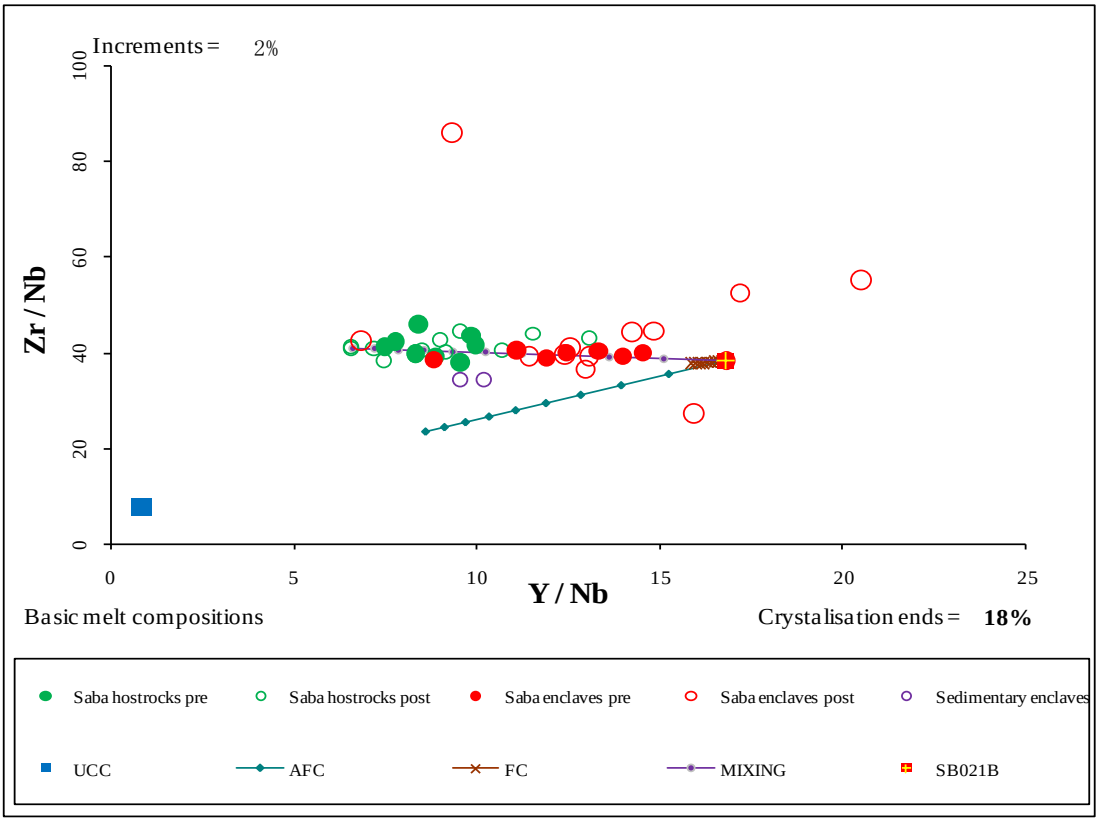

Figure 39: The data does not fit with the assimilation curve and has a very good fit with the mixing curve.

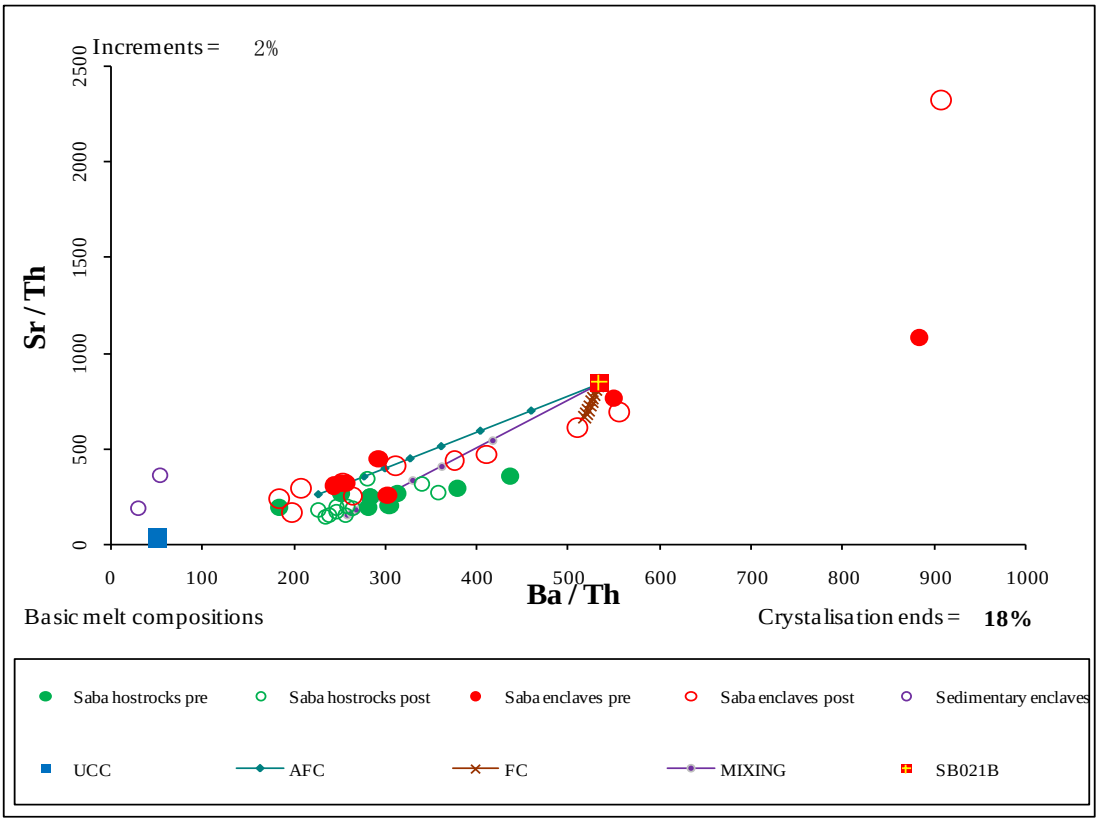

Figure 40: In this diagram both mixing as assimilation could explain the data.

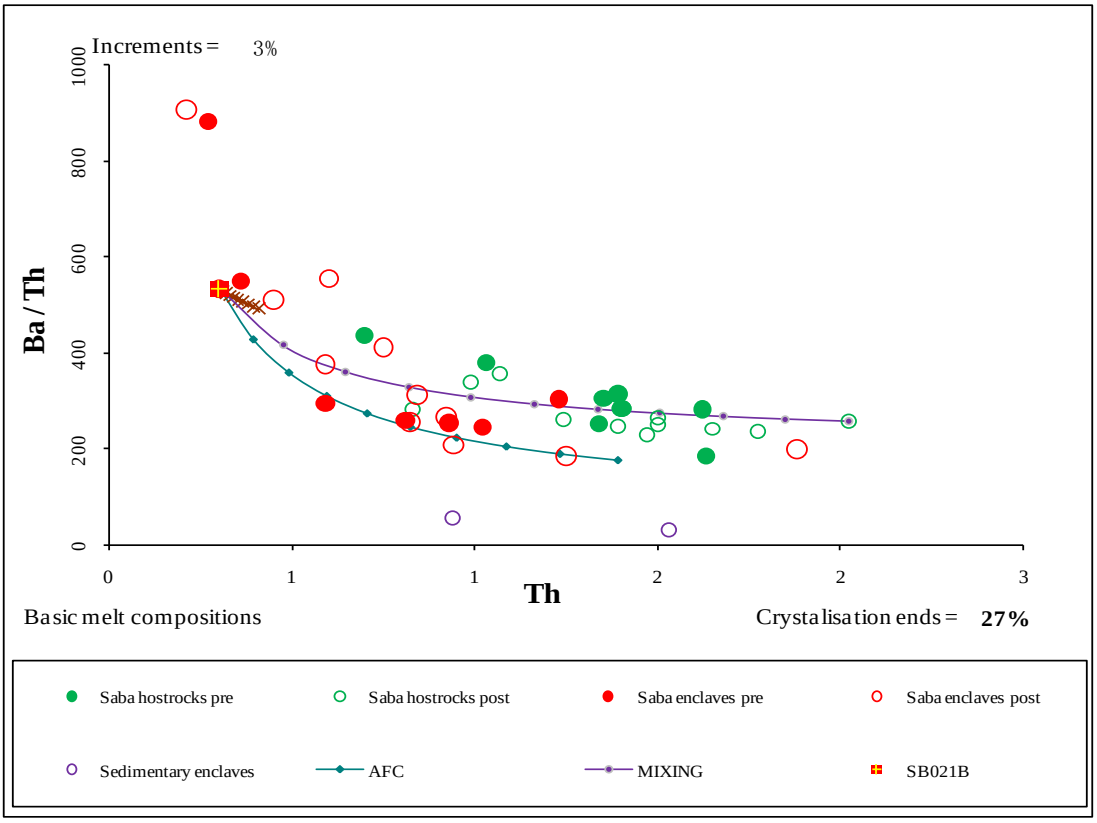

Figure 41: Although the mixing curve has a better fit with the data points, the assimilation curve also fits the data quite well and could explain the decreasing trend in the Ba/Th ratio. UCC has a Th content of 10,7 which lies beyond the scale of this diagram (Ba/Th=50,4).

Out of figure 36-41 there can be concluded that mixing is the most important differentiation process beneath Saba. Assimilation of the upper continental crust also influences the differentiation trend and certainly could explain the lowering in Ba/Th. The assimilant does probably not have an Atlantic sediment signature, but must have a MORB like $^{87}Sr/^{86}Sr$ and $^{143}Nd/^{144}Nd$ (figure 42-43). For this reason it is not likely that the UCC is the assimilant. Therefore more options are described below.

A second option could be given by the Saba Bank drill cores. Saba bank consists of four different units including sediments and (intrusive) volcanics. These units could possibly also be found underneath Saba.

A third option could be a deep volcanic arc magma (Aves Swell volcanic arc, see section 2.2) of an earlier volcanic arc which is fully crystallized and possibly altered. These rocks have a gabbroic composition with low Ba and Th contents. This option is consistent with a recently published paper of Bezard et al, 2014. In this paper osmium isotope ratios suggest that assimilation is responsible for the observed range of Os isotopic variations. They conclude that the assimilant has a MORB-like $^{87}Sr/^{86}Sr$ with high Sr (>700 ppm) and that assimilation occurred in the middle-lower crust. They suggest that the assimilant could be a plagioclase-rich cumulate which is present at the base of the arc. This cumulate could have been produced during the early-arc stage where no fluids and sediments were involved.

This third option could be provided by the rocks first interpreted (and plotted in most diagrams) as 'sedimentary enclaves'. In thin section these rocks are heavily altered and mainly consist of plagioclase with one other mineral which is possibly olivine. The barium content in these rocks is low 50,7 ppm, Sr 340 ppm. Thin section photos are shown in figure 42.

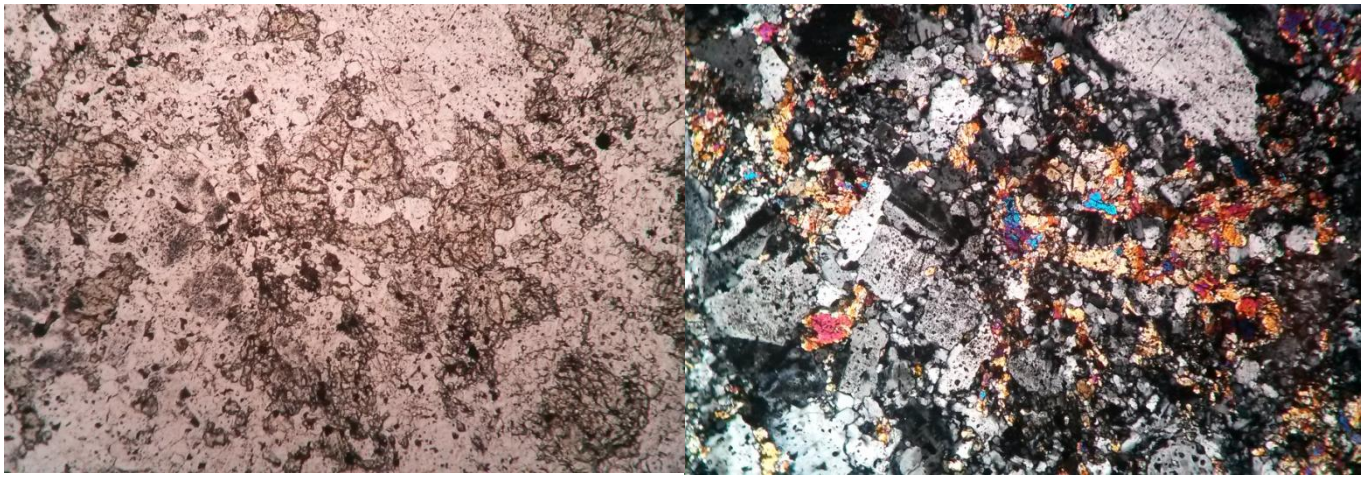

Figure 42: Thin section photos of the 'sedimentary enclaves' which is probably a early-arc stage cumulate.

5.4 The source of the mafic magma of Saba

Figure 16 and Figure 19 showed that that whole rock analysis gave higher $^{87}Sr/^{86}Sr$ values for hostrocks than for enclaves. For the plagioclase phenocrysts this distinction could not be made. The same Sr ratios for the plagioclase crystals could probably be explained by the picking process. In the picking process mostly the largest fraction of unaltered, without inclusions plagioclase phenocryst are picked. Probably this generation of plagioclases is found both in the enclaves and the hostrocks. For this reason it can be concluded that the plagioclase phenocrysts in both the enclaves and the hostrocks are derived from the same parental magma. This could possibly also explain the trend in Figure 19 where the hostrocks with higher SiO_2 values give lower $^{87}Sr/^{86}Sr$ ratios because they simply contain more large unaltered plagioclases without inclusions with the low $^{87}Sr/^{86}Sr$ ratios.

In figure 43, the data points from figure 19 are shown in comparison with $^{87}Sr/^{86}Sr$ and $^{143}Nd/^{144}Nd$ values of other islands of the Lesser Volcanic Arc, Atlantic sediments and Atlantic MORB. Note that the rocks of Saba show very unradiogenic $^{87}Sr/^{86}Sr$ and unradiogenic $^{143}Nd/^{144}Nd$, consistent with other island-arc volcanics dominated by a fluid component from the slab (e.g. Elliott et al., 1997). Compared to MORB $^{87}Sr/^{86}Sr$ shifted to slightly higher values. This can be explained by the incorporation of fluids because Sr is a large ion lithophile element (LIL). LIL elements are more mobile, particularly if a fluid phase is involved. The $^{143}Nd/^{144}Nd$ signature of Saba is comparable with MORB. This is consistent with the abundant presence of (water bearing) amphiboles in the Saba volcanics.

Figure 44 shows the Y/Nb versus Zr/Nb ratios of the Saba rocks. OIB data of the Galapagos Islands and Atlantic sediment values are added to this diagram. The MORB field is indicated by the blue area. Note that there is no variation in Zr/Nb. These values suggest that the Saba volcanics are derived from a depleted mantle source, e.g. more depleted than N-MORB. This source probably has Zr/Nb values around 30. These values can only rise to these measured ratios if more melt is extracted from this source. The high Zr/Nb also suggest that the contribution of sediment to the mantle source (with low Zr/Nb -/+14) was limited. This diagram is also consistent with the observation in isotopic data that the rocks of Saba are not influenced by sediment input.

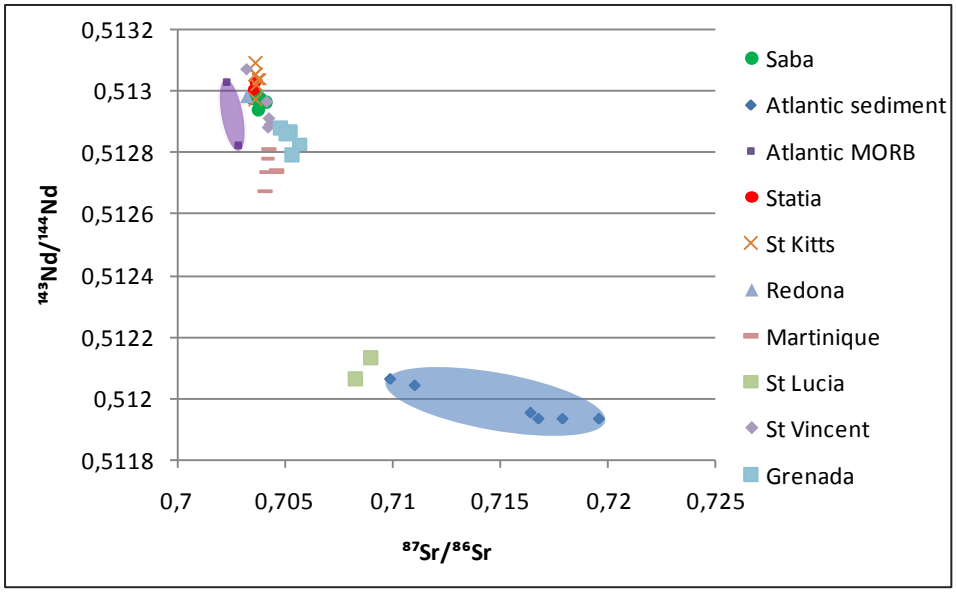

Figure 43: $^{87}Sr/^{86}Sr$ versus $^{143}Nd/^{144}Nd$ of Saba and other islands of the Lesser Antilles. Other island data obtained from Turner et al, 1996. The blue field indicates the Atlantic sediment domain and the purple field indicates the Atlantic MORB domain. Sediment data obtained from Le Roux, 1987

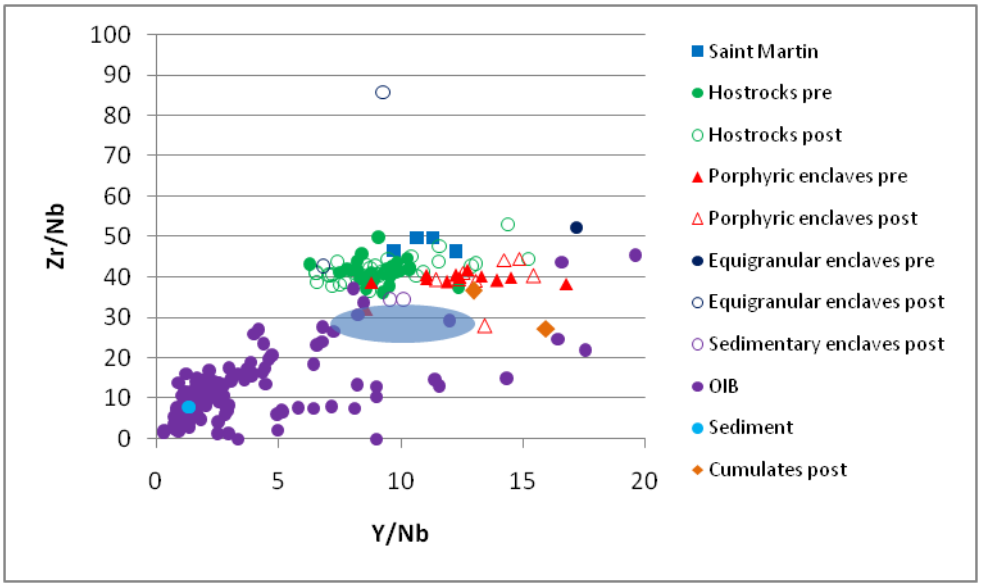

Figure 44: Zr/Nb versus Y/Nb. OIB and sediment data obtained from http://georoc.mpch-mainz.gwdg.de/georoc/ and Plank and Langmuir, 1998. MORB data obtained from Cole et al, 2007.

Another option to explain the decreasing trend in Ba/Th is that the source provides different kinds of mafic melts where at least one has a high Ba content and one has a low Ba content. Eventually these mafic melts mix.

Underneath Saba probably lies a complex magma chamber where magma mixing, fractional crystallization and assimilation all work at the same time. The main source is provided by fluid flux melting where fluids from the subducting oceanic plate work their way up. The mafic inclusions in the hostrocks indicate that the top of the magma chamber is filled with a low density felsic magma. The lower parts are filled with a higher density mafic magma. The felsic magma is probably the source of the large plagioclase phenocrysts. The altered phenocrysts could be formed at the contact between the mafic and the felsic magma where the plagioclases start to dissolute and generate their sieve textures. At the same time, new plagioclases crystallize in the mafic melt which represent the smaller phenocrysts. The observed total mixture of felsic and mafic magma at the surface is probably caused by a magma overturn where the densities of the mafic and felsic components become equal. This overturn could be caused by H_2O bubbles which cause a decrease in density in the mafic magma.

Chapter 6: Conclusions and recommendations

Abundant and clear evidence of mixing can be found on macroscopic to geochemical scale. Therefore it is clear that the geochemical composition of the Saba lavas can be explained by magma mixing of a mafic and felsic magma. The most important question in this study was to find out how the parental mafic magma differentiated to a felsic magma.

The bulk mixing equation of Langmuir was used to mix between the most mafic magma and the most felsic magma. Sample SB024AII and SB021B are seen as the most representative samples for two different sources and therefore used in bulk mixing diagrams. These diagrams show that mixing between magmas can explain a large part of the differentiation trends. The andesitic domes that compose a large part of Saba are mostly influenced by the mafic magma source. Plagioclase is the abundant mineral in SB024AII whereas amphibole is the abundant mineral in SB021B.

The felsic magma is probably derived from the mafic magma by fractional crystallization and assimilation of material from the arc crust (not sediments). This is consistent with Osmium isotope data from Bezard et al, 2014. The main minerals that crystallize are plagioclase, clinopyroxene and hornblende with minor apatite and magnetite.

Hornblende is a water bearing mineral, so the presence of this mineral also provides evidence for the presence of fluids. Saba volcanics have a slightly higher $^{87}Sr/^{86}Sr$ in comparison with MORB values. Since Sr is a LIL element this observation also indicates the presence of fluids.

Isotopic ratios of $^{87}Sr/^{86}Sr$ and $^{143}Nd/^{144}Nd$ as well as Zr/Nb ratios of Saba volcanics suggest that the influence of subducted sediment is limited (<1%). Zr/Nb values also suggest that the Saba volcanics are derived from a depleted mantle source.

$^{87}Sr/^{86}Sr$ isotopic ratios of plagioclase show that the largest unaltered fraction of plagioclase which is found in both hostrocks as in mafic enclaves all have the same source.

Some field observations could be related to increasing magmatic activity below Saba and gasses which are forcing their way up. Therefore it is recommended to start a monitoring program for Saba especially because the main village of Saba, called the Bottom is located in a valley.

References

Bezard, R., Schaefer, B.F., Turner, S., Davidson, J.P. and Selby, D., 2014, *Lower crustal assimilation in oceanic arcs: Insights from an osmium isotopic study of the Lesser Antilles.* Geochimica et Cosmochimica Acta, v. 150, p. 330-344.

Bouysse, P., and Westercamp, D., 1990, *Subduction of Atlantic aseismic ridges and Late Cenozoic evolution of the Lesser Antilles island arc*: Tectonophysics, v. 175, p. 349-380.

Cole, R.B., Layer, P.W., Hooks, B., Cyr, A., Turner, J., 2007, *Magmatism and deformation in a terrane suture zone south of the Denali fault, northern Talkeetna Mountains, Alaska:* Special Paper 431, The Geological Society of Amerika.

DePaolo, D.J., 1981, *Trace element and isotopic effects of combined wallrock assimilation and fractional crystallization:* Earth and Planetary Science Letters 53, 189-202.

Elliott, T., Plank, T., Zindler, A., White, W. and Bourdon, B., 1997, *Element transport from slab to volcanic front at the Mariana arc:* Journal of Geophysical research, v. 102, p. 14991-15019.

Germa, A., Quidelleur, X., Labanieh, S., Chauvel, C. and Lahitte, P., 2011, *The volcanic evolution of martinique island: Insights from K-Ar dating into the Lesser Antilles arc migration since the Oligocene*: Journal of Volcanology and Geothermal Research, v. 208, p. 122-135.

Le Roux, A.P., Dick, H.J.B., Gulen, L., Reid, A.M., Erlank, A.J., 1987, *Local and regional heterogeneity in MORB from the Mid-Atlantic Ridge between 54.5°S and 51°S: Evidence for geochemical enrichment*: Geochimica et CosmochimicaActa, v. 51, p. 541-555.

Langmuir, H., Vocke, R.D., Hanson, G.N. Hart, S.R., 1977,*A general mixing equation with applications to Icelandic basalts*: Earth and Planetary Science Letters 37, 380-392.

Macdonald, K.C., Holcombe, T.L., 1978,*Investigations of magnetic anomalies and sea floor spreading in the Cayman Trough*: Earth and Planetary Science letters, v. 40, p. 407-414.

Macdonald, R., Hawkesworth, C.J. and Heath, E., 2000, *The Lesser Antilles volcanic chain: a study in arc magmatism*: Earth-Science Reviews, v. 49, p. 1-76.

Plank, T., Langmuir, C.H., 1998, *The chemical composition of subducting sediment and its consequences for the crust and mantle*: Ghemical Geology, v. 145, p. 325-394.

Rollinson, H., 1993. *Using Geochemical data: evaluation, presentation, interpretation*. Pearson Prentice Hall, Harlow.

Roobol, M.J. and Smith, A.L., 2004*, Volcanology of Saba and St. Eustatius, Northern Lesser Antilles*: Royal Netherlands Academy of Arts and Sciences.

Roobol, M.J. Wright, J.V., and Smith, A.L., 1983, *Calderas or gravity-slide structures in the Lesser Antilles arc?*: Journal of Volcanology and Geothermal Research, v. 19, p. 121-134.

Taylor, S.R., McLennan, S.M., 1995, *The geochemical evolution of the continental crust*: Reviews in Geophysics, v. 33, p. 243-254.

Turner, S., Hawkesworth, C., Calsteren, van, P., Heath, E., Macdonald, R., and Black, S., 1996, *U-series isotopes and destructive plate margin magma genesis in the Lesser Antilles*: Earth and Planetary Science Letters, v. 142, p. 191-207.

Wadge, G., and Shepherd. J.B., 1984, *Segmentation of the Lesser Antilles subduction zone*: Earth and Planetary Science letters, v. 71, p. 297-304.

Warner, A.J., 1990, *The Cretaceous age sediments of the Saba Bank and their Petroleum potential*: Transactions 12th Caribbean Conference, (St. Croix, 1989), p. 341-354.

Westbrook, G.K., Maufrett, A., Munschy, M., Jackson, R., Bijou-Duval, B., Mascle, A., and Ladd, J.W., 1984, *Depth to acoustic basement and depth to intermediate horizons*: Ocean Margin Drilling Program Regional Atlas Series, Marine Science International.